SYNTHESIS, MECHANICAL AND CHEMICAL, CHARACTERIZATION OF VANADIUM- BASED AEROGELS

By

HABEL GITOGO CHURU

Bachelor of Science Mechanical Engineering Technology

Oklahoma State University

Stillwater Ok 74078

1999

Bachelor of Science Mechanical Engineering

Oklahoma State University

Stillwater Ok 74078

2004

Submitted to the Faculty of the
Graduate College of the
Oklahoma State University
in partial fulfillment of
the requirements for
the Degree of
MASTER OF SCIENCE
December, 2009

SYNTHESIS, MECHANICAL AND CHEMICAL,

CHARACTERIZATION OF VANADIUM BASED

AEROGEL

Thesis Approved:

Dr. Hongbing Lu

Thesis Adviser

Dr. Ronald D. Delahoussaye

Dr. Kaal Kalkan

Dr. A. Gordon Emslie

Dean of the Graduate College

ACKNOWLEDGMENTS

I would like to thank Dr. Hongbing Lu for serving as a thesis adviser and for continued support and advice on this project. I am grateful for the opportunity he gave me to work with a lot of the graduate students and post doctorial students in his group and benefit from the wide range of knowledge and experience in various aspects of experimental sciences and engineering. I would also like to thank Dr. Ronald D. Delahoussaye and Dr. Kaal Kalkan for accepting to serve in my thesis committee.

I would also like to thank Dr. Nicholas Leventis and his research group at Missouri University of science and Technology for his help in chemistry related part of this work, both experimental as well as theoretical.

Finally I would like to acknowledge the support of my parents, brothers and sisters as well as my wife Ann during the course of my studies at OSU.

This thesis consists of the following Papers for Publication.

1. H. Luo, **G. Churu**, H. Lu, J. Schnobrich, A. M. Hobbs, E. F. Fabrizio, A. Dass, S. Mulik, N. Leventis , *Physical, Chemical and Mechanical Characterization of Isocyanate-Crosslinked Vanadia Aerogels Journal of Sol-Gel Science and Technology*, v 48, n 1-2, p 113-134, November 2008, *Special Issue: 14th International Sol_Gel Conference, Part II*

2. Leventis, N. ; Sotiriou-Leventis, C.; Mulik, S.; Dass, A.; Schnobrich, J.; Hobbs, A.; Fabrizio, E.F.; Luo, H.; **Churu, G**.; Zhang, Y.; Lu, H.; *Polymer nanoencapsulated mesoporous vanadia with unusual ductility at cryogenic temperatures. Journal of Materials Chemistry*, v 18, n 21, p 2475-2482, 2008

Under the License # 2320241378569. See Page 62 for details.

TABLE OF CONTENTS

LIST OF TABLES

Table Page

LIST OF FIGURES

Figure Page

CHAPTER I

INTRODUCTION

Monolithic aerogels are highly mesoporous materials that have low density, low thermal conductivity, low dielectric constant as well as high acoustic impendence, a few of the properties that make them attractive for wide range of applications in thermal and acoustic insulation, electronics, separations and catalysis. However, fragility, hydrophilicity, as well as the requirement for drying using supercritical fluid extraction has limited the actual use to only specialized space applications or as Cerenkov radiation detectors in some types of nuclear reactors.

Recently, the fragility problem was solved by casting a conformal polymer coating over the skeletal framework of typical silica aerogels prepared via a base-catalyzed sol-gel method (Leventis et al. 2002). That framework consists of a pearl-necklace like three-dimensional assembly of nanoparticles. The applied polymer coating cross-links the nanoparticles by developing covalent bonding with their surface and reinforces the structure without clogging the pores. Thus, the density typically increases by a factor of 3, while the strength at failure increases by a factor of 300 with a remaining porosity at 70% (Leventis et al. 2002; Zhang et al. 2004; Bertino et al. 2004). Cross-linked samples are able to deform by over 77% compressive strain without developing surface cracks, and remain stable when saturated with water.

In an effort to explore the limits of the technology, the surface of the skeletal nanoparticles was modified with amines, which became the point of departure for

exploring cross-linking with several polymeric systems, for example with isocyanate-derived polyurethane/polyurea, epoxides and styrene (Meador et al. 2005; Katti et al. 2006; Ilhan et al. 2006; Capadona et al. 2006). In addition to the strength, other desirable properties were also introduced into the material such as hydrophobicity with polystyrene cross-linked aerogels (Ilhan et al., 2006). Nevertheless, data showing that strength-wise makes no much difference which polymeric system is used for cross-linking. That has been attributed to the fact that the gain in strength is related to the bond energy in the polymeric tethers connecting the skeletal nanoparticles, and for a more or less similar amount of cross-linker (i.e., amount of accumulated polymer) the total bond energy does not vary dramatically from one polymer to another (Leventis, 2007a). At that point, the next logical step was that strength could probably be improved further by varying the network morphology (Woignier et al. 1998); in other words, it was reasoned that different network morphologies could dissipate load-forces more efficiently, increasing strength further. For this, one approach could be to move away from silica or other metal and semi-metal oxide aerogels with pearl-necklace like nanostructures where interparticle necks are the obvious weak points that initiate failure (Leventis et al, 2007b). In this context, it is known at least since the 1940s that vanadia sol-gel derived materials consists of fibers (Livage, 1991), or perhaps even entangled worm-like nano-objects showing a 3D structure with morphology akin to the walls of a bird's nest (Sudant et al, 2004). Mechanically, vanadia aerogels appear to be brittle (Woignier and Reynes, 1998). However, after cross-linking, the interlocking of elongated worm-like objects seems to become responsible for unique mechanical properties at both room and cryogenic temperatures, which is the focus of this work.

Thus, following procedures described previously for silica and rare earth aerogels (Leventis et al. 2002; Leventis et al., 2007); we have applied an isocyanate-derived polyurethane/polyurea coating on the skeletal framework of vanadia wet gels. Directed accumulation of the polymer is templated by the hydroxyl functionality found on the surface of the vanadia nanoworms. The resulting composites were dried into aerogels with CO_2 taken out supercritically. Crosslinked vanadia aerogels (X-VOx) were characterized for their chemical, physical, morphological and mechanical properties. Specifically, the latter were studied by using dynamic mechanical analysis (DMA) and compression testing under both quasi-static conditions and high strain rates. At high strain rates subject to armor applications, we used a long split Hopkinson pressure bar (SHPB) developed at Oklahoma State University. The deformation and failure of samples at two different densities were observed with ultra-high speed photography. The deformation field was studied using the digital image correlation method (DIC) via analysis of a sequence of images under high strain rate loading. Mechanical properties were investigated with samples of different bulk densities as well as with moisture saturated samples and samples having their mesopores filled with water. Finally samples were also cooled with liquid nitrogen and stiffness, strength and ductility were investigated at cryogenic temperatures both at low moderate and high strain rate. Overall, due to the low density, it was observed that t the mechanical properties of X-VOx far surpass those of general engineering polymer especially at cryogenic structure application in terms of special mechanical properties for applications ranging from armor to cryogenic liquid storage tanks.

CHAPTER II

REVIEW OF LITERATURE

2.1 Aerogels: A Brief History and Applications

Aerogels were first prepared by Steven K. Kistler in 1931 in an attempt to prove that a Solid gel and wet gel were similar in that they both contained a continuous network of solid particles of the comparable shape and size. To prove this, he needed to find a way to remove the liquid solvent from the wet gel without damaging the solid network of the particles. The main obstacle that he encountered was that as the liquid receded during evaporation, a liquid--vapor interface was created which produced strong surface tension forces within the pores. This surface tension forces caused the pores to collapse and thus destroying the solid network of particles. This was the case when wet gel was allowed to dry in ambient air, there was severe shrinkage followed by extensive cracking. It was therefore not possible to produce solid monoliths. With this short coming, Kistler theorized that:

> *"Obviously, if one wishes to produce an aerogel, he must replace the liquid with air by some means in which the surface of the liquid is never permitted to recede within the gel. If a liquid is held under pressure always greater than the vapor pressure, and the temperature is raised, it will be transformed at the critical temperature into a gas without two phases having been present at any time." (S. S. Kistler, J. Phys. Chem. 34, 52, 1932).*

The key to successful production of aerogel was supercritical extraction of the liquid solvent in the wet gel. The process of supercritical fluid extraction is described below.

2.2 Supercritical Drying

The process of supercritical fluid extraction involves holding the solvent fluid under pressure that is greater than its vapor pressure. The temperature is then raised which results in pressure rise as well and at the critical temperature, the solvent is transformed into a gas without the creation of liquid—vapor interface. The gaseous phase could then be vented out. Initially, early pioneers in the field used alcohol as the solvent but it was a dangerous operation due to the high pressures and temperatures involved before reaching supercritical situations. A safer method was desired and was developed by introducing liquid CO_2 that was exchanged for any other solvent that would otherwise require more severe conditions.

2.3 Basic theory of SCF

By holding a fluid and keeping it at a pressure and temperature above its critical point is referred to as supercritical fluid. At this phase, regardless of the applied pressure, the pure gaseous part of the solvent cannot be liquefied as long as it is maintained above the critical temperature and pressures.

For this work CO_2 was used because of its low cost, non-toxicity and the fact that it does not react with aerogels. In addition, it has a low critical value of 31°C and 73.8 bars (about 1050Psi) for the temperature and pressure respectively.

During supercritical drying, liquid CO_2 is introduced into a high pressure chamber (autoclave) where wet samples are and it replaces the liquid solvent trapped inside the pores of the samples. In the case of both the templated aerogels and vanadium based aerogel which were investigated, the liquid solvent used was acetone, while acetonitrile was the pore—filling solvent used to prepare base catalyzed silica aerogels. Once all the liquid solvent has been replaced by liquid CO_2, the pressure in the chamber was rapidly increased to a point where it is above the critical point of CO_2. It is important to avoid a situation where both the liquid and vapor are present at the same time because the receding surface of the fluid would introduce strong surface tension forces that would course the pores to collapse. The idea is to ensure that the high pressure chamber is taken through a rope around the critical point.

2.5 State of the Art in Aerogel Production

Monolithic aerogels are highly mesoporous materials that have low density, low thermal conductivity, low dielectric constant as well as high acoustic impendence, a few of the properties that make them attractive for wide range of applications in thermal and acoustic insulation, electronics, separations and catalysis. However, fragility, hydrophilicity, as well as the requirement for drying using supercritical fluid extraction has limited the actual use to only specialized space applications or as Cerenkov radiation detectors in some types of nuclear reactors.

Recently, the fragility problem was solved by casting a conformal polymer coating over the skeletal framework of typical silica aerogels prepared via a base-catalyzed sol-gel method (Leventis et al. 2002). That framework consists of a pearl-necklace like three-dimensional assembly of nanoparticles. The applied polymer coating cross-links the nanoparticles by developing covalent bonding with their surface and reinforces the structure without clogging the pores. Thus, the density typically increases by a factor of 3, while the strength at failure increases by a factor of 300 with a remaining porosity at 70% (Leventis et al. 2002; Zhang et al. 2004; Bertino et al. 2004). Cross-linked samples are able to deform by 77% compressive strain without developing surface cracks, and remain stable when saturated with water.

In an effort to explore the limits of the technology, the surface of the skeletal nanoparticles was modified with amines, which became the point of departure for exploring cross-linking with several polymeric systems, for example with isocyanate-derived polyurethane/polyurea, epoxides and styrene (Meador et al. 2005; Katti et al. 2006; Ilhan et al. 2006; Capadona et al. 2006). In addition to the strength, other desirable properties were also introduced into the material such as hydrophobicity with polystyrene crosslinked aerogels (Ilhan et al., 2006). Nevertheless, data showing that strength-wise makes no much difference which polymeric system is used for cross-linking. That has been attributed to the fact that the gain in strength is related to the bond energy in the polymeric tethers connecting the skeletal nanoparticles, and for a more or less similar amount of cross-linker (i.e., amount of accumulated polymer) the total bond energy does not vary dramatically from one polymer to another (Leventis, 2007a). At that point, the next logical step was that strength could probably be improved further by varying the

network morphology (Woignier et al. 1998); in other words, it was reasoned that different network morphologies could dissipate load-forces more efficiently, increasing strength further. For this, one approach could be to move away from silica or other metal and semi-metal oxide aerogels with pearl-necklace like nanostructures where interparticle necks are the obvious weak points that initiate failure (Leventis et al, 2007b). In this context, it is known at least since the 1940s that vanadia sol-gel derived materials consists of fibers (Livage, 1991), or perhaps even entangled worm-like nano-objects showing a 3D structure with morphology akin to the walls of a bird's nest (Sudant et al, 2004). Mechanically, vanadia aerogels appear to be brittle (Woignier and Reynes, 1998). However, after cross-linking, the interlocking of elongated worm-like objects seems to become responsible for unique mechanical properties at both room and cryogenic temperatures, which is the focus of this work.

Thus, following procedures described previously for silica and rare earth aerogels (Leventis et al. 2002; Leventis et al., 2007), we have applied an isocyanate-derived polyurethane/polyurea coating on the skeletal framework of vanadia wet gels. Directed accumulation of the polymer is templated by the hydroxyl functionality found on the surface of the vanadia nanoworms. The resulting composites were dried into aerogels with CO_2 taken out supercritically. Crosslinked vanadia aerogels (X-VOx) were characterized for their chemical, physical, morphological and mechanical properties. Specifically, the latter were studied by using dynamic mechanical analysis (DMA) and compression testing under both quasi-static conditions and high strain rates. At high strain rates subject to armor applications, we used a long split Hopkinson pressure bar (SHPB). The deformation and failure of samples at two different densities were observed

with ultra-high speed photography. The deformation field was studied using the digital image correlation method (DIC) via analysis of a sequence of images under high strain rate loading. Mechanical properties were investigated with samples of different bulk densities as well as with moisture saturated samples and samples having their mesopores filled with water. Finally samples were also cooled with liquid nitrogen and stiffness, strength and ductility were investigated at cryogenic temperatures both at low moderate and high strain rate. Overall, due to the light density, it is are clearly visible that the mechanical properties of X-VOx far surpass those of general engineering polymer especially at cryogenic structure application in terms of special mechanical properties for applications ranging from armor to cryogenic liquid storage tanks.

CHAPTER III

METHODOLOGY: SAMPLE SYNTHESIS AND EXPERIMENTS

3.1 Materials Used

Vanadium (V) tripropoxide was purchased from Sigma Aldrich (Milwaukee, WI) and used as received. Acetone was obtained from AAPER Alcohol and Chemical Co. (Shelbyville, KY). Desmodur N3200 hexamethylene diisocyanate was donated courtesy of Bayer Corporation (Pittsburgh, PA). Deionized water was produced using a Millipore Milli-Q water system and purified to 18.2MΩ. Siphon grade CO_2 was obtained from BOC Gases, Murray Hill, NJ, supplied locally by Ozarc Gases. The molds for cylindrical samples appropriate for compression testing were 10ml polyethylene syringes (Luer-LokTM Tip, BD 10 ml); the molds for square cross-section samples for three point bending were square glass tubes (ACE Glass Incorporated, Vineland, NJ, part No. 8700-91, SP/4 10mm ID); and, molds with an 8mm × 3mm rectangular cross section for Dynamic Mechanical analysis were custom-made by ACE Glass.

3.2 Sample Preparation and Drying

Vanadia wet gels were prepared by copolymerization of a vanadium (V) tripropoxide solution in mixture of acetone and water, which is a modification of Dunn's procedure (Chaput et al., 1995). In a typical process, two solutions, solution A containing 5.58 ml of

de-ionized water (0.310 mol), 11.34 ml of acetone (0.155 mol), and solution B containing 2.4 ml of vanadium(V) tripropoxide (0.0106 mol) were cooled in an acetone/dry ice bath until ice appeared in solution A; solution B just became more viscous. Solution A was vigorously shaken until all chunks of frozen water/acetone disappeared, and at that point it was added into solution B rapidly all at once. The dark orange-red mixture (sol) was shaken vigorously for 10-15 s and it was poured directly into molds where it quickly turned to green. The synthesis protocol is as shown in figure 1.

Square and rectangular cross-section molds were open at both ends; one end was covered with two layers of Parafilm, and the sol was poured from the other end, which was then also covered with two layers of Parafilm. Gelation occurred in about one minute while the sol was still cold. Samples were left in their molds to age for five days. After that period, gels were removed from the molds and were placed in a large jar with fresh acetone, approximately 4-5 times the total volume of the gels. The contents of the jar were agitated periodically, and acetone was changed four times, once every 24 h. Native vanadia (VOx) aerogels were obtained by a final solvent exchange in an autoclave where the pore filling acetone was replaced with liquid CO_2, which was then taken supercritical and was vented off isothermally (Zhang et al., 2004; Katti et al., 2006).

Alternatively, acetone-exchanged wet gels were cross-linked by reaction with a Desmodur N3200 solution in acetone. For this, the fourth acetone wash was replaced by an equal volume of a solution containing 32.9 g Desmodur N3200 in 82 mL of acetone. The jar was then swirled gently after 24 hours and gels were allowed to remain in the crosslinking bath for 36 hours. The concentration of Desmodour N3200 in the bath was

varied resulting in crosslinked aerogels with different densities. Subsequently, gels were heated in an oven at 50 °C for 72 hours under two different conditions: either in the crosslinking bath or in fresh acetone. Typically, crosslinked vanadia (X-VOx) aerogels cured in acetone have lower densities than X-VOx aerogels cured in the crosslinking bath. After 72 hours, gels were removed from the oven and they were washed four more times with fresh acetone. Finally they were dried with CO_2 taken out supercritically as in the case of the native samples.

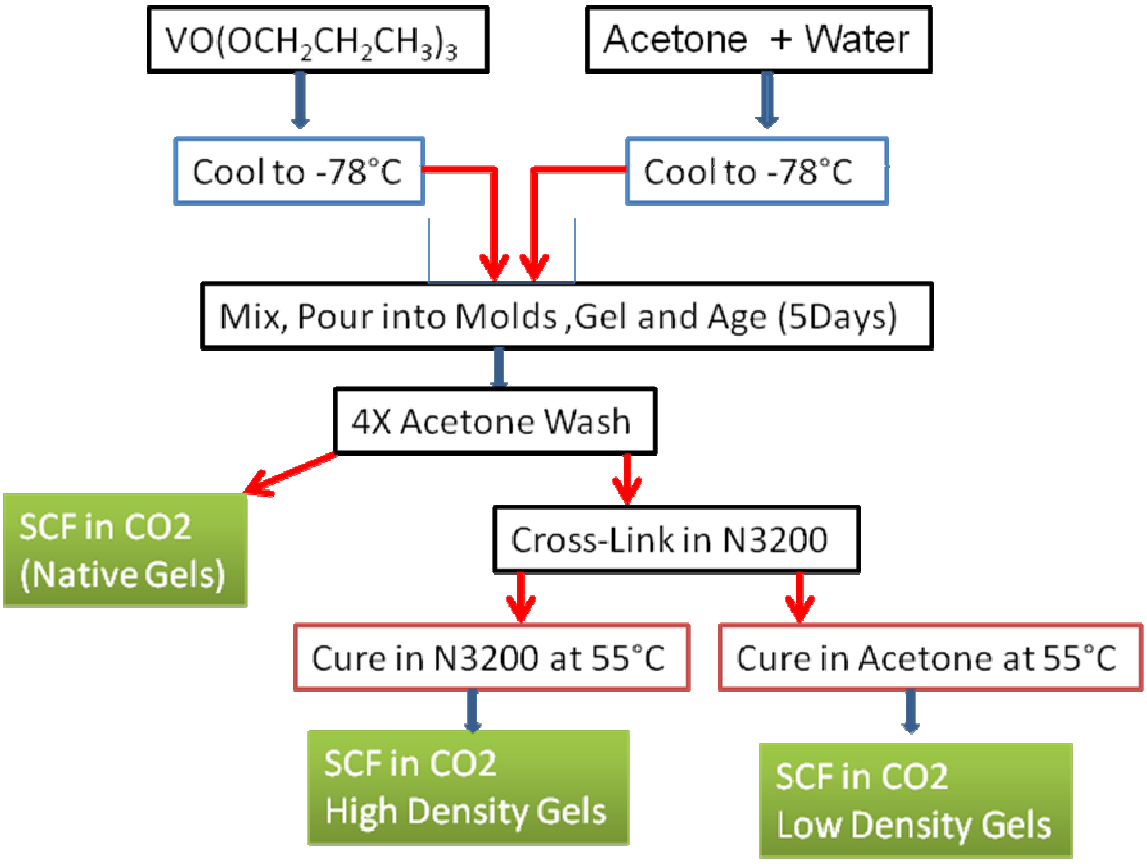

Figure 1: Flow chart of Vanadium aerogel making protocol

3.3. **Thermal, Physical and Chemical Characterization**

Thermal characterization was conducted by thermogravimetric analysis (TGA) and differential scanning calorimetry (DSC). TGA was performed on a TA Instruments Model 2950 HiRes instrument at 10 $^{\circ}$C/min under nitrogen. DSC was conducted with a TA Instruments Model 2010 apparatus also at 10 $^{\circ}$C/min under nitrogen.

The aerogel nanostructure was characterized by scanning electron microscopy (SEM) and nitrogen sorption porosimetry. For SEM, samples were coated with Au and were observed with a Hitachi S-4700 field emission microscope. For nitrogen sorption porosimetry samples were outgassed at 80 $^{\circ}$C for 24 h, and were analyzed with an ASAP 2000 Surface Area/Pore Distribution analyzer (Micromeritics Instrument Corp.). Porosity, as percent empty space, was calculated from bulk and skeletal density data; the latter were obtained by helium pycnometry using a Micromeritics AccuPyc 1330 instrument.

Chemical characterization was performed by XRD, XPS, infrared and attenuated total reflectance (ATR) infrared spectroscopy. For XRD, samples were looked at in the continuous mode with a Phillips X'Pert Materials Research Diffractometer (model PW3040/60) using Cu Kα radiation (λ=1.54 Å). The incident beam prefix module was an X-ray mirror (PW3088/18) equipped with a sealed proportional detector (PW3011/20). XPS was conducted on a KRATOS AXIS 165 XPS Spectrometer equipped with a magnesium anode at 225W, using an electron pass energy of 20 eV. A Nicolet Nexus 470 FT-IR spectrophotometer was used to obtain both infrared spectra of powder samples in

KBr pellets, as well as ATR infrared spectra across the radius of disks cut from larger monoliths.

3.4 Uni-axial Quasi-static Compression Test:

Cross-linked vanadia (X-VOx) have a nano-fibrous structure coated conformally with a nano-layer of polymer. However, their relative rigid walls lender them to physically behave like rigid plastics. For that reason, quasi-static compression tests were done in accordance to ASTM standard D 695—02a which is technically equivalent to ISO 604. The main reason for this test was to find such critical data about the samples such as the compressive strength, compressive yield strength, and Young's modulus. In addition, the data obtained was used to calculate the specific energy of material, which was obtained by calculating the area under the stress—strain curves.

ASTM standard D 695—2a prescribes that the length to diameter ratio of the samples be 2:1 for tests on rigid plastics. Samples with circular cross-section were prepared using 10ml syringes as mold material as described above. After the samples were dried, they were cut to size with a diamond saw and the tool marks left by the sow were removed using a fine grade sand paper and also polish the sides of samples. This ensured that there was no stress concentration on the scratches left by the tool marks left during machining.

Figure 2: Test specimen set on test platens of MTS test machine before Compression test

Quasi-static tests were done at room temperature, -5°C, at -50°C and at cryogenic temperatures of about -180°C. For tests at -5˚C, samples were left in the fridge for six hours. The platens of the compression machine were then cooled by placing ice on them before the samples were placed there. Tests were then carried out within ten seconds from the start of the test to the finish. For test at -50˚C, the samples were placed in dry ice obtained from a liquid carbon dioxide tank with a dip tube in it. The temperature of the dry ice was measured to be about -70˚C. Just like in the case of the tests at -5˚C, dry ice was placed on the platens to cool them before the tests were carried out. Finally, for tests at -180˚C, the samples were wrapped in aluminum foil and then dipped in liquid nitrogen for six hours. There after they were taken out of the liquid nitrogen, unwrapped and placed on the platen where a steady flow of nitrogen was maintained to make sure that there was no significant rise in temperature during the test. All other test conditions were maintained the same as for room temperature tests.

One of the limiting factor for wide spread use of aerogel is their hydrophilicity. Previous work by Leventis at al [2] showed that it could be reduced by applying a conformal

polymer layer on the mesoporous surface of the aerogel secondary particles. The effect of water on the mechanical properties was then investigated by submerging test specimens in water for thirty days. Measurements and weight of the samples were taken after every eight hours for the first two days and then in two day intervals till there was no significant change in both the dimension as well as the weight. They were then tested as described above using ASTM D 695—2a standard as described in previous tests.

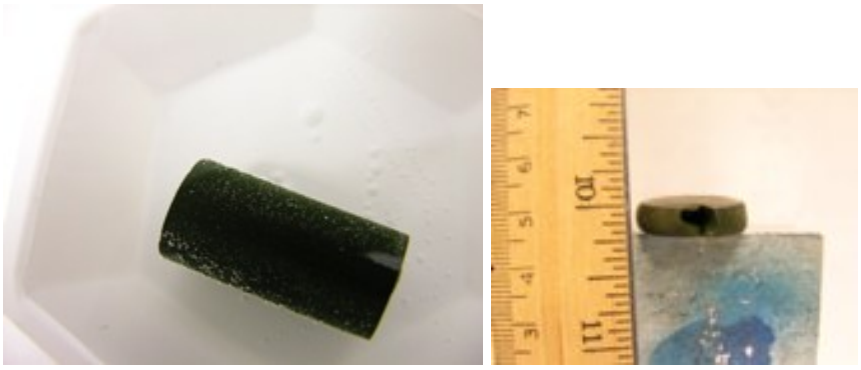

Figure 3: Compression samples in water before and after the test

Tests were also carried out at different strain rates achieved by simply varying the cross head speed of platen. Strain rate was varied from a low of 0.001/second to a high of 1/second. This test was done at room temperature only. Finally, to determine how the material handles repetitive loading, the samples were subjected to load and unload compression tests. Standard specimens with a ratio of 2:1 for length to diameter ratio were used as prescribed by the ASTM D 695—2a standard were loaded by bringing the test platen together to compress the samples to a pre-determined strain and then the motion of the platen was reversed to unload.

3.5 Dynamic Mechanical Analyses (DMA)

Complex modulus was investigated using 55mm long, 13mm wide and 2mm thick specimens prepared using glass molds as described above. A model RSA II dynamic mechanical analyzer (Rheumatics Scientific Inc. Piscataway, NJ) was used to conduct DMA tests at University of Oklahoma (Norman, Ok). Each sample was loaded on the knife support of the test chamber and the loading was applied at the mid-span of the sample which now behaved as a simply supported beam as shown in the diagram. A load of 10 grams was introduced at the mid-span to make sure that the sample was always in contact with the knife-loading fixture when oscillating load was applied. The frequency was set at 1Hz and then liquid nitrogen was introduced into the chamber to cool the sample to the lower limit of -122°C while the upper temperature limit was set at 250°C. Data sampling was then set at every two minutes and the sample was soaked for 20 seconds before recording the data. The loss modulus, the storage modulus as well as tan delta were all recorded simultaneously at each temperature set.

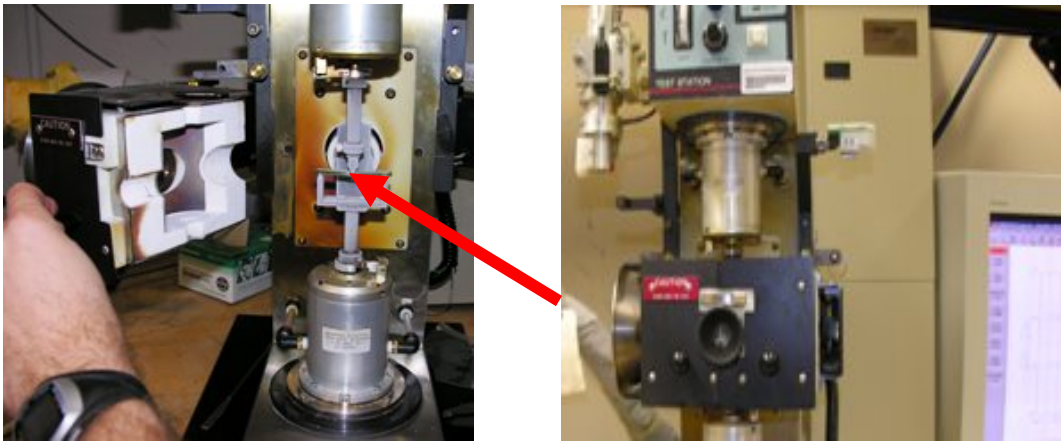

Figure 4: Vanadium aerogel sample resting on DMA machine test chamber

3.6 Compressive Experiments at High Strain Rates

Compressive experiments at high strain rates of 50-2500 s^{-1} were conducted under ambient condition at room temperature 23 ± 1◦C and under relative humidity 35 ± 3%, using on a long split Hopkinson pressure bar (SHPB) facility developed at Oklahoma State University. The schematic diagram of the SHPB is shown in Figure 6. The SHPB consists of a steel striker bar, incident and transmission bars, strain data acquisition system, and an ultra-high speed photography system using Cordin 550-62 ultra-high speed camera. A disk shaped X-VOx samples (13.72 mm in diameter and 2.54 mm in thickness) of two densities ware sandwiched between the incident and transmission bars. A pulse shaper was used to generate a smooth incident wave, reducing the dispersion of the incident wave due to the bar geometry (Frew et al., 2002). A hollow transmission bar was used to reach high signal-to-noise ratio for the transmitted signal. Prior work by Chen's group (Chen and Zhang, 1999; Chen and Lu, 2002) determined that the wave dispersion under 1-D wave propagation is negligible when appropriate pulse shaping is used. The incident and transmission bars made of 304L stainless steel had lengths 7514 and 4049 mm, respectively, with an outer diameter equal to 19 mm. The inner diameter of the transmission bar was 14.1 mm. At the end of the transmission, a cap end made of hard tool steel was press-fitted into the hollow tubing to support the specimen. An appropriate pulse shaping can remove the end cap effect on 1D stress wave propagation (Chen and Zhang, 1999). A new pulse shaper, consisting either a metal tubing placed inside another one, or two pieces of copper tubing, was used to help reach dynamic stress equilibrium state and constant strain rate, necessary for a valid SHPB experiments. The working principle of SHPB has been well documented in literature (Gary, 2000; Gama

and Lopatnikov, 2004). Under a valid SHPB experiment, formulas for the history of stress, strain rate and strain in a specimen have been also documented (Luo, Lu and Leventis 2006). In the case of high strain rates, SHPB experiments were all determined the effect of strain rate, water, moisture, absorption, and low temperature. In each SHPB experiment, three or more specimens were tested to assure repeatability under the same test conditions.

Figure 5: SHPB set up at Oklahoma State University

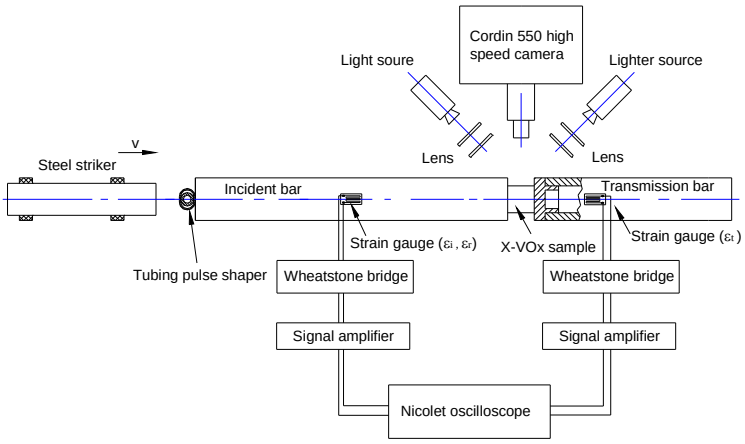

Figure 6: Schematic of the SHPB set up and various components

3.7 High-speed Photography and Digital Image Correlation

A Cordin 550-62 high speed digital camera (62 color frames, up to 4 million frames per second, 10-bit resolution CCD with 1000 × 1000 pixels) was used to acquire images of a specimen at a rate of 71,829 frames per second. Two Cordin 605 high intensity Xenon light sources with two sets of lenses were used to illuminate the specimen surface. In order to reach good focus, cubic specimens 10.4mm on the edge were used. The use of such specimens allowed the measurement of Poisson's ratio and the observation of the failure. A speckle pattern was printed on the surface facing the camera using black silicon rubber dots. The silicon rubber coating is so soft with Young's modulus of about 1 MPa that the strengthening effect is negligible. Also it was determined that the rubber does not react with the X-VOx. Digital image correlation (DIC), a non-contact full-field deformation measurement method widely used to measure surface deformations (Knauss and Zhu, 2002; Luo, Lu and Leventis, 2006), was used to measure surface deformations on specimens. In DIC, two images, the reference image and the deformed image, are

compared to determine the surface deformations through tracking distinct gray scale patterns. In this work, the DIC code developed by Lu and Cary (2000), capable of measuring both first-order and second-order displacement gradients, was used to determine the surface deformations on a specimen.

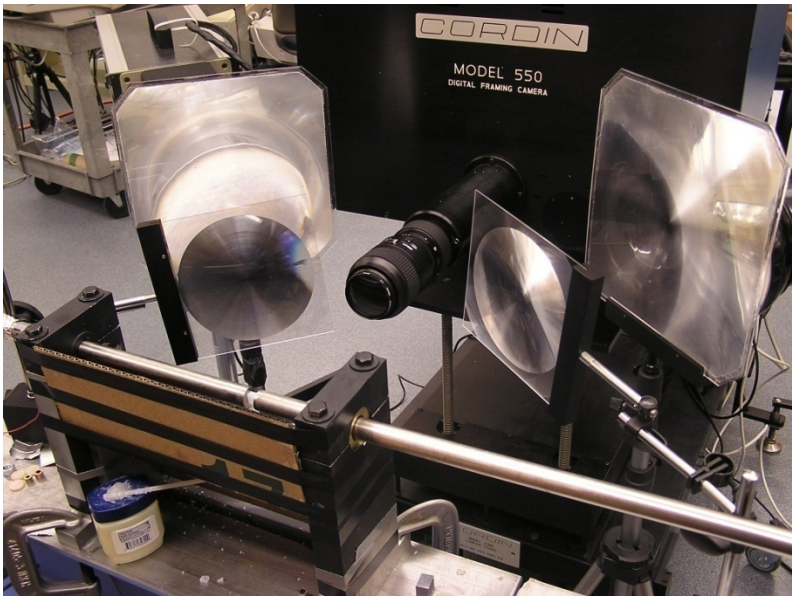

Figure 7: High speed setup at the SHPB test site

3.8 Effects of Density, Water and Moisture Absorption, and Low Temperature

The mechanical behavior of X-VOx aerogel depends on their mass density. The effect of density on the stress-strain relationship was investigated at a strain rate of ~ 300 s^{-1}. Since X-VOx has open-cell nanoporous structure, it can absorb water and moisture. Experiments were conducted to determine the effect of water and moisture absorption on the compressive behavior at high strain rates. Water-soaked samples were prepared by immersing dry X-VOx samples into water allowing them to absorb water to reach fully saturated state. In order to investigate the effect of moisture, samples were stored under

97% relative humidity for about two months in an enclosed container (desiccator). The mass and volume changes were also monitored during this period. The weight change was measured with a balance (Denver Instrument, APX-200, max 200 g) with resolution of 0.1 mg. After two months, X-VOx aerogels had reached a moisture saturation state. Both water-soaked and moisture fully saturated X-VOx specimens were used to measure the stress strain relation at a strain rate of ~ 330 s^{-1}. Results are compared with those from dry X-VOx specimens at room temperature.

A refrigerator was used to cool samples to -5°C; dry ice was obtained from CO2 tank with a dip tube and the temperature was measured be about -72°C and samples were placed in a vacuum flask to cool them and temperature at test time was about -50 °C; liquid N_2 (melting point -197 °C) in a Dewar were used for reaching cryogenic temperature (-170 °C). All samples were kept at the set temperature for at least 6 hours to reach thermal equilibrium. For SHPB experiments, once samples were ready for testing, they were placed quickly between the incident and transmission bars and the testing was completed within 2~3 seconds.

CHAPTER IV

FINDINGS

4.1 Synthesis, Physicochemical and Morphological Characterization of Vanadia Aerogels

Vanadia aerogels (VOx) were prepared by supercritical fluid (SCF) CO_2 drying of corresponding wet gels, which in turn were prepared by modification of Dunn's procedure (Chaput et al, 1995) whereas vanadyl triisopropoxide was substituted with vanadyl tripropoxide; the latter had been used in earlier protocols (Livage, 1991). The substitution was essential for our purposes, because invariably all large monolithic gels prepared via the former vanadium source developed cracks even while still in their molds. Figure 1 schematically summarizes the preparation procedures for both native as well as polymer cross-linked samples. Cooling of the acetone/water solution and the vanadium tripropoxide sample slows gelation which otherwise takes place upon mixing, and gives time to pour the mixture into the molds. Aging for five (5) days is important, because it strengthens the wet gels enough for gentle handling. Wet gels were solvent-exchanged by four acetone washes and they were either dried to produce native vanadia aerogels (VOx) or they were subjected to a cross-linking process as described below.

Table 1 summarizes key properties of these materials. Macroscopically, native vanadia aerogels are green, suggesting the presence of vanadium(IV), and consistently with the literature (Chaput et al, 1995) they are highly porous (consisting of ~97% empty

space), low-bulk density materials (~0.08 g/cm^3) which are also extremely fragile. Their BET surface areas are around 216 m^2/g, which are closer to those reported for vanadia ambigels obtained by ambient pressure drying rather than for aerogels (~300 m^2/g) prepared via SCF drying (Sudant et al, 2004). Microscopically, they consist of entangled 100-200 nm long, 30-40 nm thick worm-like objects shown in Figure 3(A) whose surface morphology reminds the surface morphology of secondary particles of silica aerogels (Katti et al., 2006), suggesting that they are also formed by coalescing primary particles. By closer examination of SEM images shown in Figure 3(A) the size of the primary particles seems to fall in the 6-8 nm range. XRD shown in Figure 4(A) of a native vanadia aerogel shows a nanocrystalline material with well defined, albeit broad, reflections at 2θ =26.37° and at 2θ=50.58°. From the half-width of the XRD reflections we calculate (via the Scherrer method) that the crystallite size is in the range of 5 nm (derived from the peak at 26.37 degrees) and 12 nm (derived from the peak at 50.58 degrees). On one hand this broad particle size range reflects a disorganized solid, but on the other hand it matches with the primary particle size estimated from SEM shown in Figure 3(A).

The best match for the observed reflections in XRD is for $V_3O_7.H_2O$, implying that vanadium (V) was reduced during processing (probably by acetone) to vanadium (IV). The presence of vanadium (IV) is quantitatively supported by the XPS data shown in Figure 9 (B) showing a broad vanadium $2p_{3/2}$ peak with a shoulder at lower binding energies indicating the presence of both the 5^+ and 4^+ oxidation states (Dutoit et al, 1997). Thus assuming two peaks, both with 80% Gaussian and 20% Lorentzian contributions, centered at 517.8 eV (vanadium V) and at 516.47 eV (vanadium IV), with a common

half-width of 1.6 eV, it is calculated that vanadium is present at 67.61% as vanadium(V) and at 32.39% as vanadium (IV). These data support the XRD assignment for $V_3O_7.H_2O$.

Infrared spectra of native vanadia aerogels (Figure 11-bottom, dashed line) show the strong absorption of V=O at ~1000 cm^{-1}, while broad V-O bands appear below 900 cm^{-1}. The spectrum, however, is dominated by a broad absorption in the 3500 cm^{-1} and a second one at 1625 cm^{-1}, which are assigned to surface hydroxyls and adsorbed water (Chaput et al, 1995). The presence of adsorbed water is further indicated by TGA analysis (Figure 6) that shows a loss of ~15% mass at around 100 $^{\circ}C$ accompanied by a strong exothermic heat flow (by DSC) with a peak at 80 $^{\circ}C$.

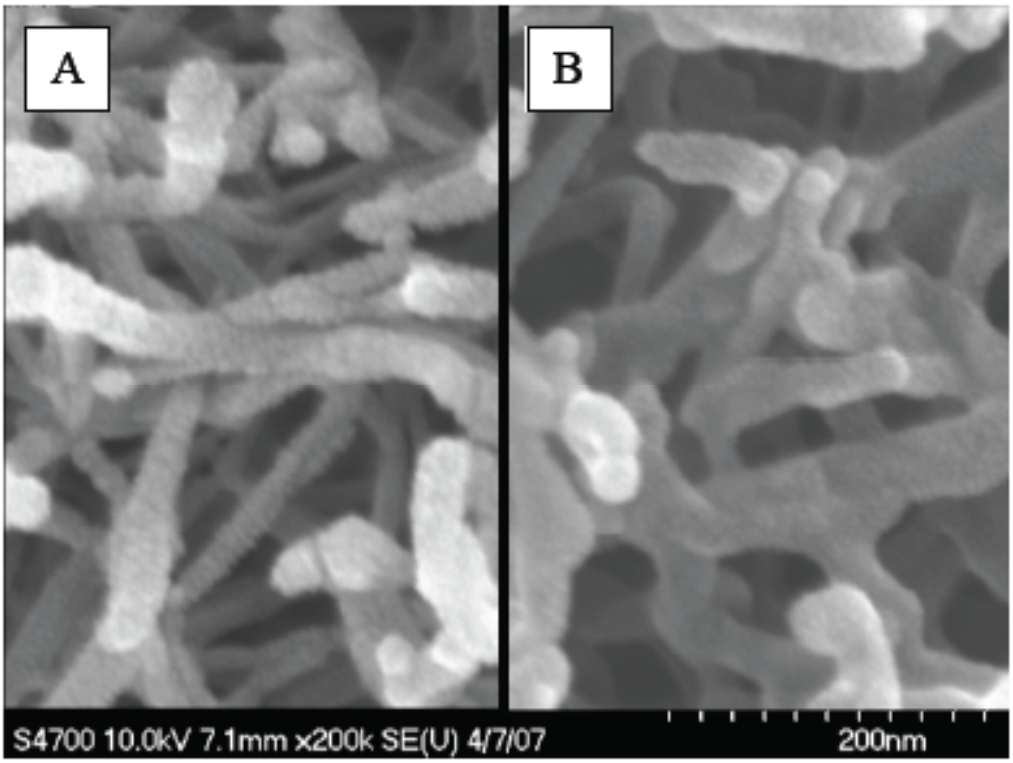

Figure 8: SEM of Vanadium aerogel

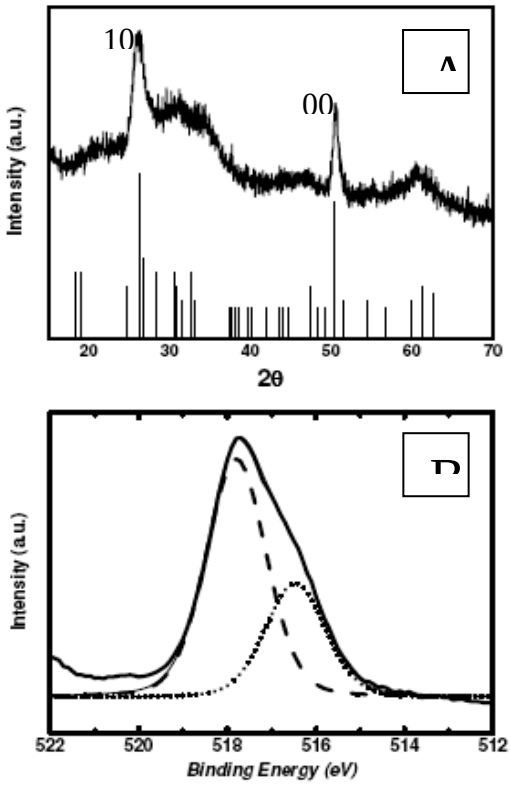

Figure 9: XPS results for vanadium Aerogels

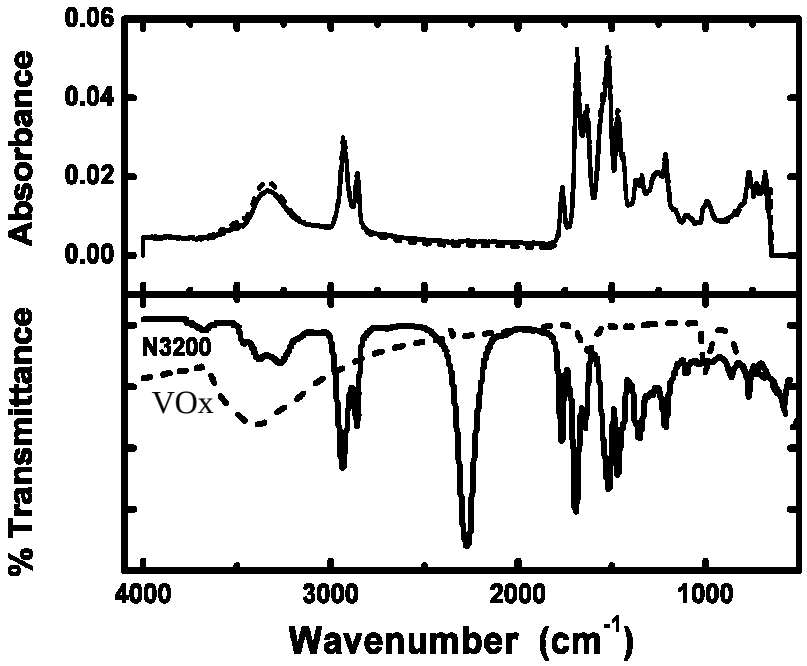

Figure 10: ATR infrared spectra near the center (solid line) and near the perimeter (dashed line) of a crosslinked vanadia aerogel (X-VOx) disk (~2 diameter) cut off a larger monolithic cylinder. Bottom: IR of a native vanadium aerogel (VOx, ρ_b=0.078 g/cm^3, dashed line) and of neat Desmodur N3200.

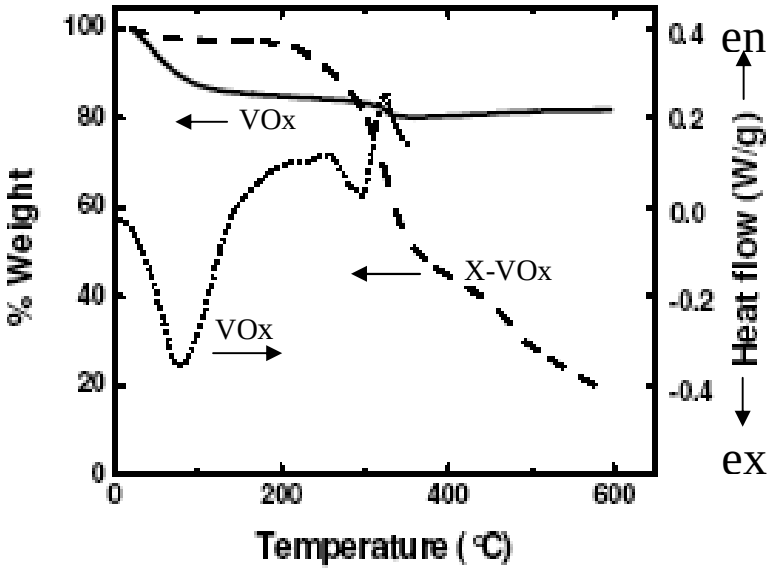

Figure 11: TGA and DSC results

The presence of adsorbed water is essential for building interparticle tethers. Thus, in analogy to our recent investigations with silica and rare earth aerogels, vanadia wet gels are expected to react with isocyanates introduced in the mesopores, developing interparticle molecular tethers via formation of: (a) urethane groups by reaction with hydroxyl groups on the surface of vanadia, and (b) urea bridges with other isocyanates from the mesopores; the latter are formed by a two-step reaction sequence whereas dangling isocyanates are hydrolyzed by surface adsorbed water to yield CO_2 and dangling amines, which in turn react with free diisocyanates in the mesopores to give urea. As demonstrated in Table 1, the amount of isocyanate uptake, and therefore the density of the resulting aerogels, can be controlled by two methods: either by varying the concentration of the diisocyanate in the crosslinking bath, or by curing the isocyanate-equilibrated wet gels in the acetone/isocyanate equilibration bath itself or in fresh acetone. The resulting cross-linked vanadia aerogels (X-VOx) were characterized by

ATR-IR spectroscopy. Figure 10-top shows two spectra, one at the edge and one at the center of a disk cut with a diamond saw off a ~2 cm in diameter cylindrical X-VOx monolith. These data confirm uniform distribution of the polymer throughout the sample, and by comparison with the spectrum of neat N3200 diisocyanate (Figure 10-bottom solid line) the isocyanate stretch at ~2300 cm^{-1} has disappeared while the diazetidine dione stretch of N3200 at 1767 cm^{-1} has survived the crosslinking process in analogy to X-silica and X-rare earth aerogels (Zhang et al, 2004; Katti et al, 2006; Leventis et al, 2007). The presence of ureas in the monomer obscures the formation of new ureas by the cross-linking process, although the relative size of the feature at ~1695 cm^{-1} has increased. Now, Figure 3(B) confirms that nanoscopically, material has been taken conformally to the skeletal worm-like objects. By comparison SEM images of figure 8(B) with 8(A), the thickness of the coating for the particular cross-linked X-VOx sample is approximately 4 nm. Concurrently, the BET surface area has decreased relative to the value range of the native samples, while the average pore size has increased, reflecting restricted access to the smaller crevices on the skeletal framework by the polymer coating. The skeletal density of the cross-linked samples has also decreased relative to the skeletal density of the native samples, reflecting the weighted average density of the polymer and the underlying inorganic skeletal framework. By TGA (Figure 6) X-VOx samples contain ~3% w/w moisture, while polymer starts decomposing above 300 $^{\circ}C$, in analogy to corresponding X-silica or X-rare earth samples (Zhang et al. 2004; Katti et al. 2006; Leventis et al. 2007). The mass loss up to 600 $^{\circ}C$ indicates that the corresponding cross-linked monolith consists of ~82% of isocyanate-derived polymer. This is consistent with the density gain by cross-linking of the particular VOx samples (from 0.078 g/cm^3 to

0.421 g/cm^3) corresponding to 81% w/w polymer, and also with the skeletal density change from that of native vanadia (~2.854 g/cm^3) to cross-linked vanadia (1.293 g/cm^3, for samples cured in acetone with bulk density of 0.421 g/cm^3); indeed, considering the density of Desmodur N3200 derived polyurea (1.14591 g/cm^3), it is calculated that the skeletal density of a sample consisting of 82% polymer, 3% water and a balance of vanadia (15%) should be 1.398 g/cm^3.

Sample ID/ N3200:acetone in bath (g/mL)	Bulk Density (g/cm^3)	Skeletal Density (g/cm^3)	Porosity (%)	BET area (m^2/g) (Av. Pore diam., nm)
VOx				
Native samples	0.078±0.011	2.854±0.112	97	216 (56.5)
X-VOx: Samples cured in acetone				
5.5:95	0.219±0.009			
11:94	0.257±0.003	1.383	81	
33:82	0.421±0.008	1.293±0.015	67	99.7 (71.2)
X-VOx: Samples cured in the N3200: acetone bath				
5.5:95	0.338±0.005			
11:94	0.465±0.007	1.257	63	
33:82	0.593±0.004	1.236±0.008	52	68.4 (109)

Table 1: Results of BET analysis

4.2 Dynamic Mechanical Analysis (DMA).

Between -129 °C and 210 °C at 1 Hz, the complex modulus data (storage modulus and loss modulus) of X-VOx in acetone with density 0.465 g/cm^3 were determined. We present results in terms of nominal stress and nominal strain with reference to initial dimensions. Figure 13 shows the storage modulus, loss modulus, and loss tangent as a function of temperature. It is seen that the Young's modulus at room temperature (24°C)

is 669.6 MPa. In general, the storage modulus decreases with the increase of temperature. At -129 °C, the storage modulus is 1243 MPa; at 100 °C the modulus is reduced to 315 MPa. Around 118.4 °C, the storage modulus decreases at a steep rate, thereby indicating an α-glass transition. Above 118.4 °C, the storage modulus shows a slight increase; at 207 °C the modulus decreased to 24.3 MPa, i.e., about 19.5% of the value at -129 °C. Figure 13 further includes the loss modulus and the loss tangent, tangent of out-of-phase angle δ, $\tan\delta$, calculated in terms of the ratio of loss modulus to storage modulus. In a typical viscoelastic material the sinusoidal strain lags behind sinusoidal stress by a phase angle within $0 \sim \pi/2$. Figure 13 shows that there is a major peak in $\tan\delta$ around 118.4 °C, marked with "A". The peak corresponds to a high-to-low viscosity transition, indicating that the material undergoes softening around that temperature. This peak is consistent with the rapid reduction in the storage modulus, thus indicating the major glass transition temperature (α-transition) as 118.4 °C. It is noted that silica aerogel cross-linked with a N3200 isocyanate-derived polymer (Katti et al, 2006) have shown an α-transition at about 130 °C, indicating the proximity of glass transformation in silica and vanadia aerogel, both cross-linked with di-isocyanate-derived polymer supporting a really ideal chemical identical to materials.

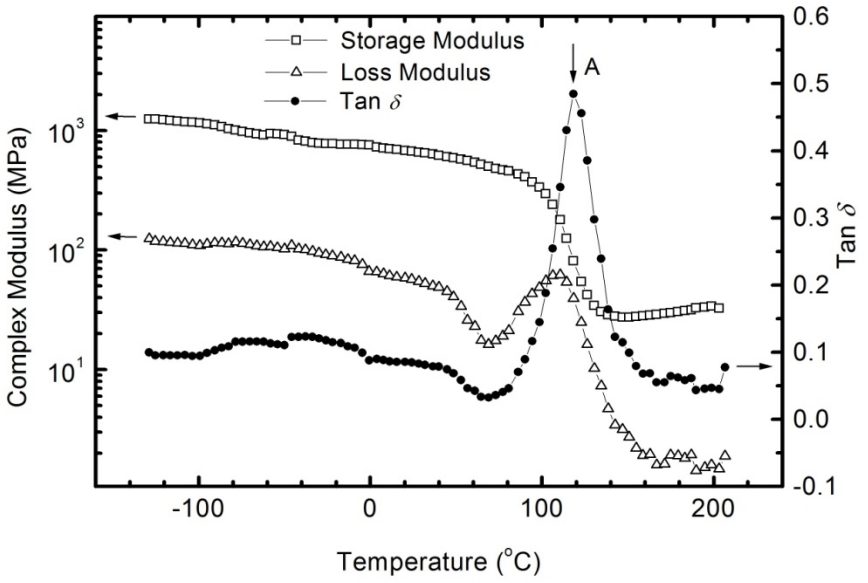

Figure 12: DMA test results showing the α-transition at point A where grass transition occurred.

4.3 Quasi-static Compressive Testing.

Figure 14 shows typical compressive stress-strain curves at 4×10^{-4} s^{-1} for native vanadia and X-VOx aerogel under unconfined conditions. Native VOx aerogel are extremely brittle, developing surface cracks that lead to fragmentation as strain rate increases. However, at very small strain rate of about 0.00005/s, we were able to compress the specimen to about 94% resulting in yield strength of about 3.2MPa and Young's modulus of about216MPa while final failure occurred at 114MPa at 87% strain. The Young's modulus E, 0.2% yield strength $\sigma_{0.2}$, ultimate compressive strength σ_b and ultimate failure strain ε_b as determined from Figure 14 are listed in Table 2.

This investigation focused on the characterization of the cross-linked vanadia aerogels that are much more ductile and stronger than their native counterpart. After cross-linking with isocyanate, the cross-linked vanadia aerogels, or X-VOx, have about 3.5 times of density of native vanadia. All compressive stress-strain curves show three stages of deformations, a linearly elastic region under small compressive strain (<4%); a yielding regime with slight hardening until 60% compressive strain; and a densification and plastic hardening range until 84% ultimate strain. It may be noted that both (native) VOx and the (cross-linked) X-VOx have similar Young's modulus and yield strength except different low strain rate. At a strain rate 5×10^{-3} s^{-1}, X-VOx cured in acetone has lower Young's modulus, yield strength and ultimate compressive strength than those of X-VOx cured in N3200. Cross-linked vanadia aerogels cured in either N3200 or acetone have much higher ultimate compressive strength than that of native VOx's. The specific energy absorption is 36.93 MPa·mm/mm for X-VOx of density 0.422 g/cm^3 under quasi-static loading. The Poisson's ratio as determined at an axial compressive strain 5% is 0.15 when the sample expands laterally in the initial compression. Samples did not buckle during quasi-static compression at room temperature. The materials are mostly absorbed within their own porosity so that lateral deformation did not show any visible increase after initial 5% compressive strain. Figure 15 shows typical X-VOx samples before and after compression testing. At failure, despite the splitting of the sample and the development of numerous cracks emanating in the radial directions, the outer layer of all cross-linked samples did not shatter and flew away, and the sample remained still single piece. The significant increase in ductility over the native vanadia aerogel can be tracked

as the polymer coating reinforces the weak connection between the fibrous nanostructures.

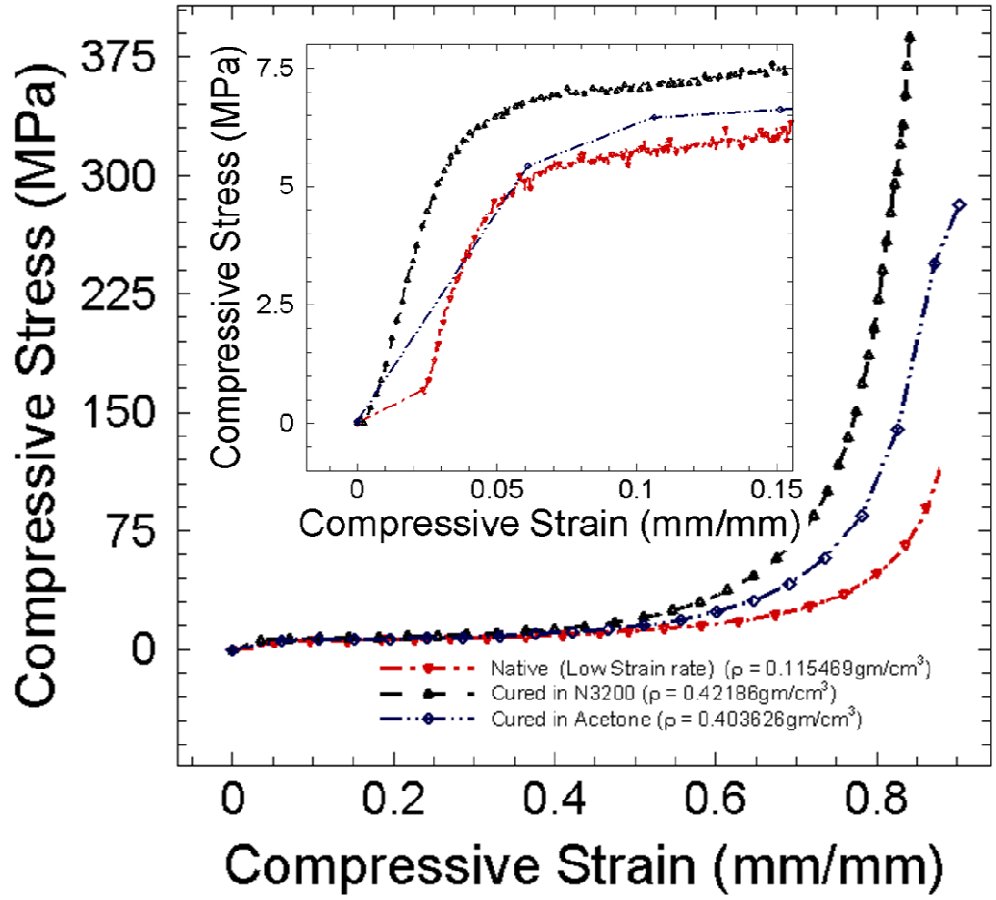

Figure 13:Compression results for various types of vanadium gels

Figure 14: Sample before and after compression test.

Figure 16 shows the stress-strain curve with seven unloading/reloading cycles. All unloading exhibited the nonlinear recovery. Unloading stiffness (slope of the unloading stress/strain curve) is negative, possibly induced by a memory effect in the polyurea coating, which exhibits the viscoelastic behavior. Prior to each unloading, there was a loading event with increase in stress and strain. At the beginning of unloading, even though the stress has started to decrease, the strain would keep increasing due to a memory effect, leading to the formation of negative slope in the initial unloading stage of each cycle. Reloading at compressive strain levels lower than 40% appear to follow loading curve starting at a stress free state. Reloading at a higher compressive strain level shows higher stiffness, induced most likely by the increase in density due to the compaction of the X-VOx. Reloading in all cases does not follow the unloading curves, resulting that hysteresis loops are seen in each unloading/reloading cycle. The unloading curve becomes steeper at higher compressive strain levels (e.g., between 68% and 76%), indicating a reduced elastic behavior for samples having experienced higher level of densification by compaction. Figure 16 also shows a curve for straight loading showing that it closely traces a path on top of the load and unload curve, an indication that the material is able to recover considerably after each loading and that the overall strength is not affected much by the loading and unloading process.

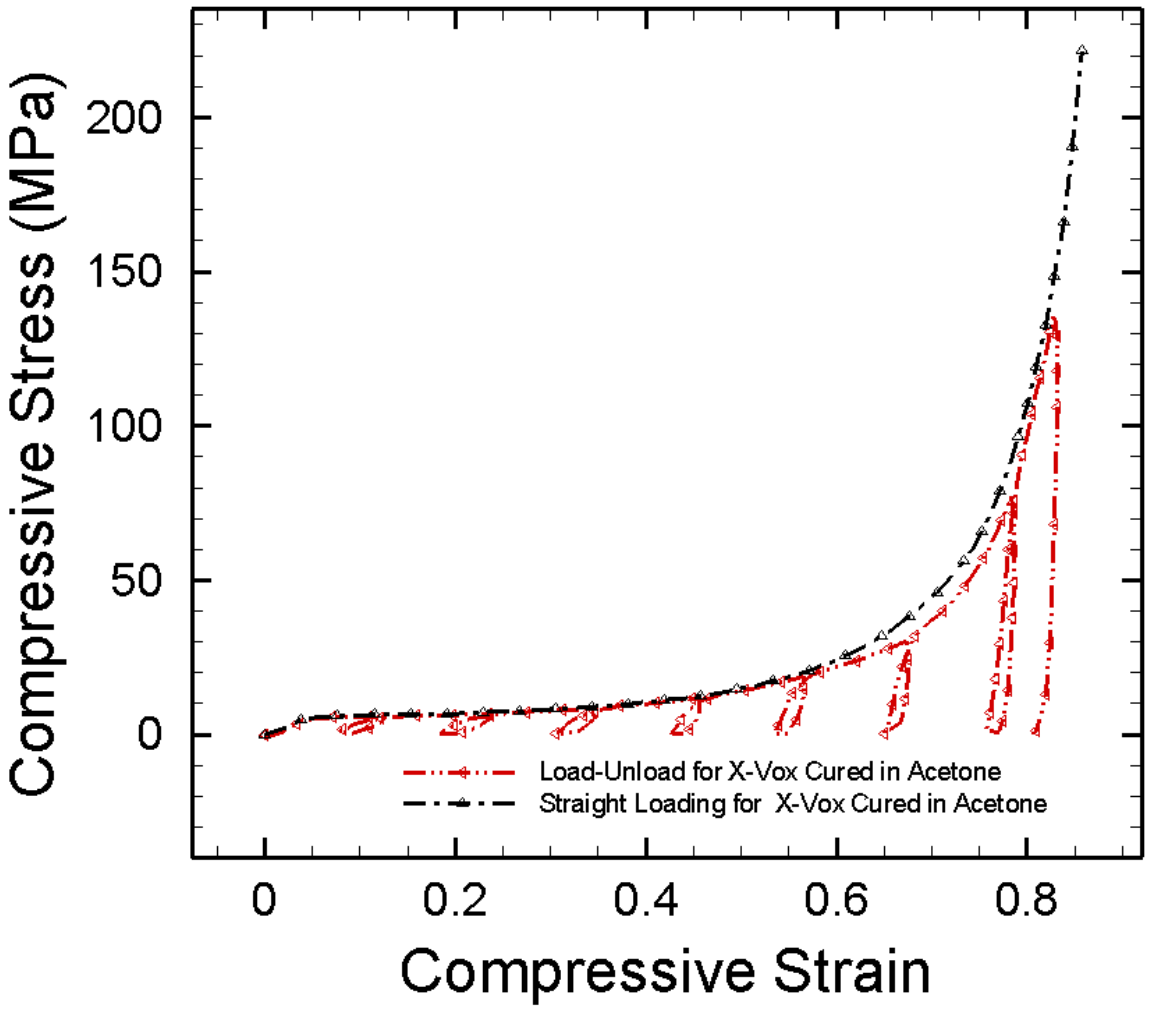

Figure 15: Comparing load-unload with straight loading for vanadium aerogel samples cured in acetone

The effect of strain rate on the mechanical behavior was first evaluated under quasi-static loading conditions. Figure 17 shows the stress-strain curves at strain rates 4×10^{-4}, 5×10^{-3}, and 4×10^{-2} s^{-1} for X-VOx cured in N3200. The Young's modulus, 0.2% offset yield strength, ultimate compressive strength and ultimate compressive strain as determined from Figure 17are also summarized in Table 2. As strain rate changes by two orders of magnitude, the overall stress-strain curves do not exhibit significant changes. These

results indicate that at these low strain rates, the mechanical behavior for X-VOx does not have a strong dependence on the strain rate. For applications such as energy absorption at high speed impact further testing at high strain rate using a split Hopkinson pressure bar would be necessary and the results are presented in next section.

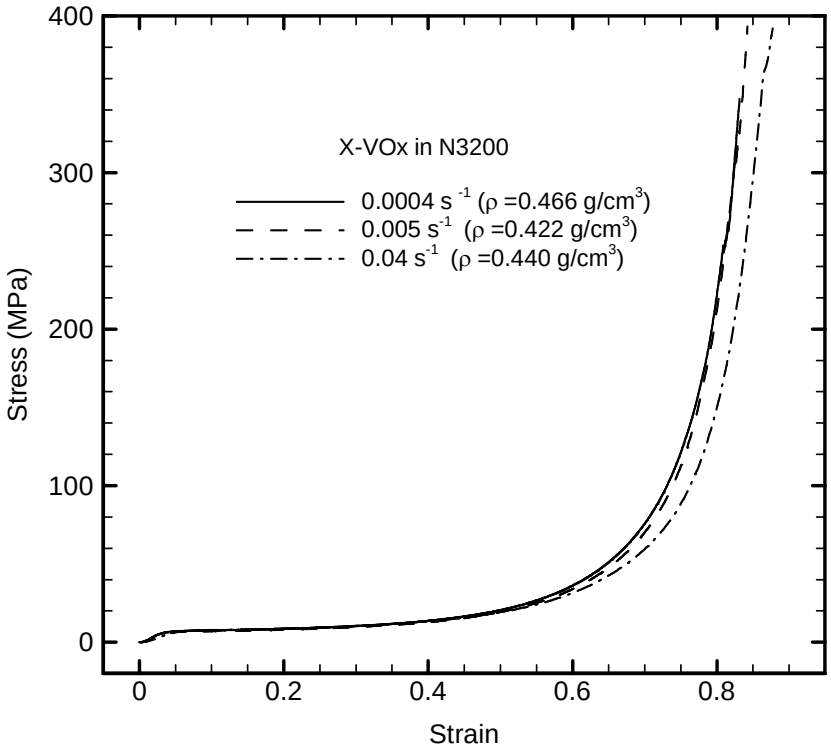

Figure 16: Quasi-static compression tests for tests at different strain rates

The effect of water absorption was investigated by comparing compressive testing results using both dry and water-soaked samples. After immersing a X-VOx sample in water for two days (the minimum time for water to saturate), the sample reached fully saturated state, and gained weight by 140% with an increase in volume less than 0.5%, indicating that water enters mostly the pores without causing the worm-like fibers to expand. Figure

17compares the stress-strain curves for both dry and water-soaked X-VOx samples at a strain rate of 5×10^{-3} s^{-1}. The Young's modulus, 0.2% yield strength, ultimate strength and strain in Figure 18 are also summarized in Table 2. The stress-strain curves as shown in Figure 17 indicate that the water-soaked sample is weaker than a dry sample. The Young's modulus, yield strength, and ultimate compressive strength of water-soaked X-VOx decreased by 20%, 43% and 64% than dry X-VOx. But remarkably, the water-soaked samples were still stable, did not dissolve in water, and were still ductile, albeit not as much as a dry sample. The water-soaked samples failed at an ultimate compressive strength of about 78.4 MPa and at an ultimate compressive strain of 83%, similar to a dry sample and are compared to dry samples in figure 17 below.

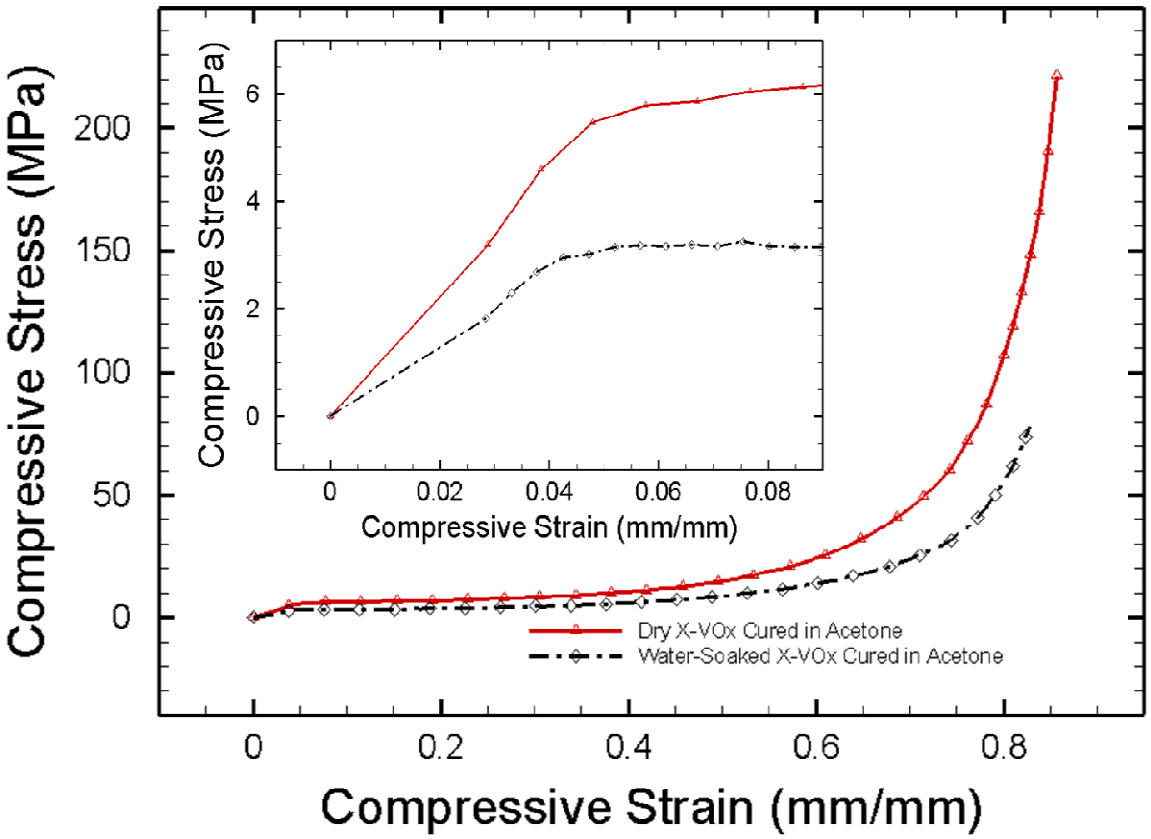

Figure 17: Compressive stress-strain curve comparing dry sample with water soaked one.

Figure 18 shows compressive results of X-VOx at low temperature at a strain rate of 0.365 s^{-1}. Such a relatively high strain rate was needed so that at low temperatures, samples were tested within a very short time, usually within 3-5second to avoid any significant temperature change. As the temperature decreases, the material becomes stiffer, and the stress-strain curve shift in generally to the above. It indicates that the X-VOx can absorb more energy at lower temperatures (-5 °C and -50°C). However, as temperature decrease to about -180 °C, the sample still remain ductile until 30% strain and the sample was broken in buckling failure. Still the area under the curve was comparable for the case of samples tested at room temperature and at -180°C, showing that the material can still absorb significant amount of energy even at cryogenic temperatures. The reason is 2:1 sample ratio between length and diameter and near moderate strain rate 0.365 s^{-1}, indicating that the ratio should be reduced in SHPB testing under the high strain rate.

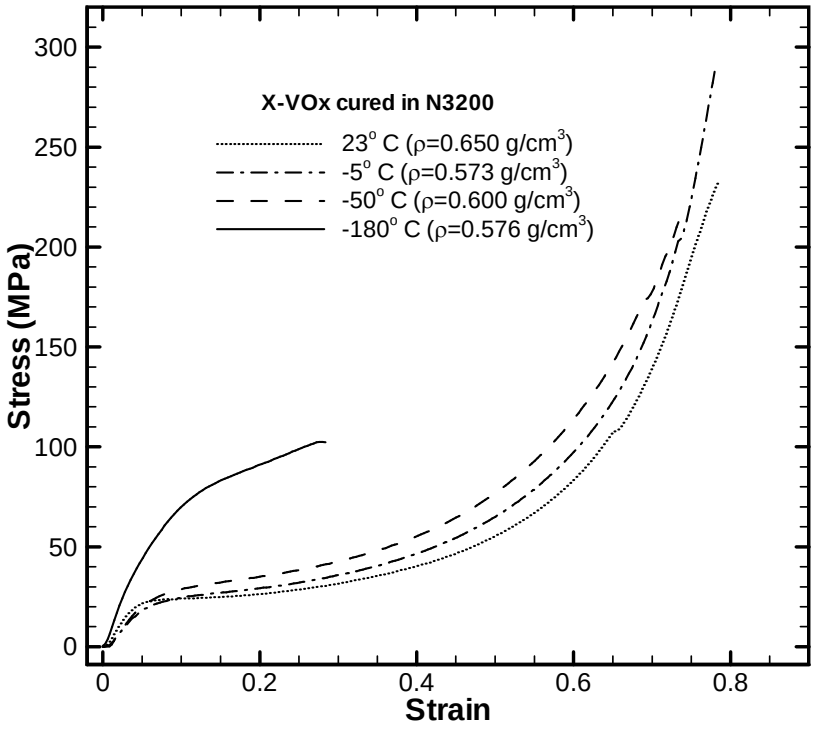

Figure 18: Compressive stress strain curves at different temperature.

Overall, for static compression, X-VOx with density of 0.422 g/cm^3 has an average yield strength of 5.22 MPa, an ultimate compressive strength within 240-370 MPa, and ultimate compressive failure strain as high as 84%. The specific energy absorption, indicated by the area enclosed by the in stress strain curve, is 36.93 MPa·mm/mm, indicating that X-VOx is especially suitable for force protection such as for energy absorption in automobile collision and armor applications.

Materials	ρ (g/cm^3)	Strain rate (s^{-1})	E (MPa)	σ_y (MPa)	σ_b (MPa)	ε_b	Dry or Water
Native VOx	0.115	0.0004	215.8	3.73	114.3	0.86	Dry
X-VOx in acetone	0.404	0.005	159.5	5.02	222.2	0.84	Dry
X-VOx in N3200	0.422	0.005	225	5.21	225.3	0.84	Dry
X-VOx in N3200	0.466	0.0004	287.0	5.08	347.0	0.83	Dry
X-VOx in N3200	0.422	0.005	217.5	5.29	393.0	0.84	Dry
X-VOx in N3200	0.440	0.04	179.0	5.61	292.0	0.88	Dry
X-VOx in acetone	0.415	0.005	155.2	5.12	220.3	0.85	Dry
X-VOx in N3200	0.996	0.005	124.0	2.94	78.4	0.83	Water

Table 2: Summary data for quasi-static compression tests

4.4 Compression at High Strain Rates using SHPB

We next present results on X-VOx obtained using a long split Hopkinson pressure bar. In a SHPB test, the dynamic equilibrium state, indicated by equal stresses applied on both ends of the specimen, must be established. Such an experiment is then considered valid and the acquired experimental data are processed to the dynamic stress-strain relations. To examine the dynamic equilibrium condition, as following the 1-wave (transmitted wave), 2-wave (difference between incident wave and reflected wave) method (Gary, 2000; Gama and Lopatnikov, 2004), the front stress (the end of specimen in contact with the incident bar) and back stress (the end of specimen in contact with the transmission bar) on the specimen are compared, as a function of time and depicted in Figure 20, as well as the strain rate history.

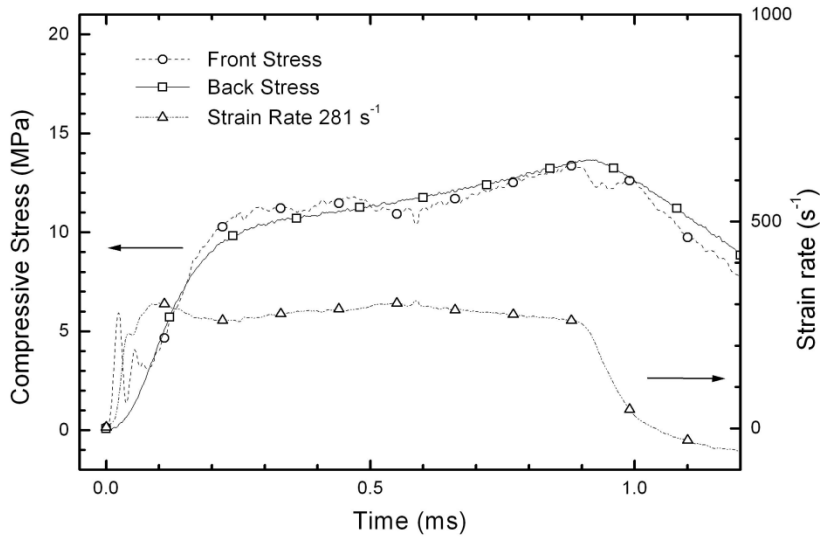

Figure 19: Dynamic stress equilibrium check and constant strain rate of X-VOx

The front stress is very close to the back stress, indicating that the dynamic equilibrium condition was nearly established and the specimen was nearly uniformly deformed except during the initial 100μs rising-up stage. By the pulse shaping, the strain rate is nearly flat during most of the loading stage with only a slight variation (~2.5%), indicating that the specimen deformed approximately under a constant strain rate. Then the incident, transmitted and reflected signals were processed further to determine the stress-strain relation at high strain rates.

4.5 Effect of Strain Rate

The compressive stress-strain curves for X-VOx under unconfined conditions at several strain rates within the 50 s^{-1}-2500 s^{-1} range are shown in Figure 20. In general at these high strain rates X-VOx samples are linearly elastic under small strains (<3%). Then they

yield at ~3% compressive strain and exhibit plastic hardening until ~50% strain under uniform compaction. Subsequently, X-VOx samples are densifies and fail at ultimate compressive strain of 60-70%. Since the length of the bar allows loading for 1.5 ms, at a medium strain rate, the attainable maximum strain within 1.5 ms was lower than that at a higher strain rate. Consequently, at medium strain rates, the specimen remained unbroken during experiments so that the compressive stress-strain curves shown in Figure 20 are not the complete curves, which was the limit for SHPB experiments with available limited length of metal bars. This situation happened to curves at strain rates 50, 70, 281, and 334 s^{-1} in Figure 20. At strain rates above 1000 s^{-1}, all samples failed so the compressive stress-strain curves shown are complete. The X-VOx sample becomes stiffer as the strain rate increases. Thus, the mechanical behavior of X-VOx depends highly on high strain rate.

Figure 21 shows the SEM images before and after SHPB testing for X-VOx with density 0.424 g/cm^3. The original X-VOx nano-structure exhibit a nano-porous skeletal frameworks with a fibrous (worm-like), and 3-D order nanowire stacking together morphology, very similar to the way a bird nest are constructed and the remaining space between the skeletal fibers to form the mesoporosity, as shown in Figure 21. After SHPB impact at 60% plastic strain under strain rate $1200s^{-1}$, most of nanopores disappeared and the skeletal X-VOx material, vanadia skeletal fiber plus the polymer coating, was compacted together. Also the size of the skeletal X-VOx nano-fibers had become thicker and larger, and a part of polymer coating which links fibers had been fused together to become a large piece during high strain rate and large strain loading condition. This

interested phenomenon was not interpreted now according recent available physics theory, which remains future research if applicable.

Both the Young's modulus data and the 0.2% offset compressive yield strengths are plotted in Figure 22 as a function of strain rate. The yield strength increases with the strain rate. The relationship between yield strength and strain rate is fitted to the literature models (Chen, 1998) and given by equation 1,

$$\frac{\sigma_y}{\sigma_0} = 1 + \frac{2}{\pi} C_1 \tanh\left[\ln\left(\frac{\dot{\varepsilon}}{\dot{\varepsilon}_0} \right)^{m_1} \right] \qquad (1)$$

where σ_y is the 0.2% offset compressive yield strength; σ_0 is a reference compressive strength; $\dot{\varepsilon}_0$ is the reference strain rate; C_1 and m_1 are constants. As seen in Figure 22, this model can describe the yield data reasonably well. The Young's modulus increases also with the strain rate. The threshold strain to reach dynamic stress equilibrium is ~2%, corresponding to 100 μs rising-up time. The Young's modulus data are considered to be valid as the dynamic equilibrium state was established below the limit of linearity. Following the relationship established for cross-linked silica aerogels (Luo, Lu and Leventis, 2006), the Young's modulus is given as a function of strain rate in the form of equation 2,

$$\frac{E}{E_0} = C_2 \left(1 + \ln\left(\frac{\dot{\varepsilon}}{\dot{\varepsilon}_0} \right)^{m_2} \right) \qquad (2)$$

where E_0 is the referred Young's modulus; C_2 and m_2 are constants. From the experimental data, the best-fit constants C_1, C_2, m_1 and m_2 are summarized in Table 3.

This model can also describe the experimental data very well, as seen in Figure 22. The specific energy absorption values are 26.84 and 39.73 MPa·mm/mm for X-VOx at densities 0.424 g/cm^3 and 0.576 g/cm^3, respectively, at a strain rate of ~2400 s^{-1}.

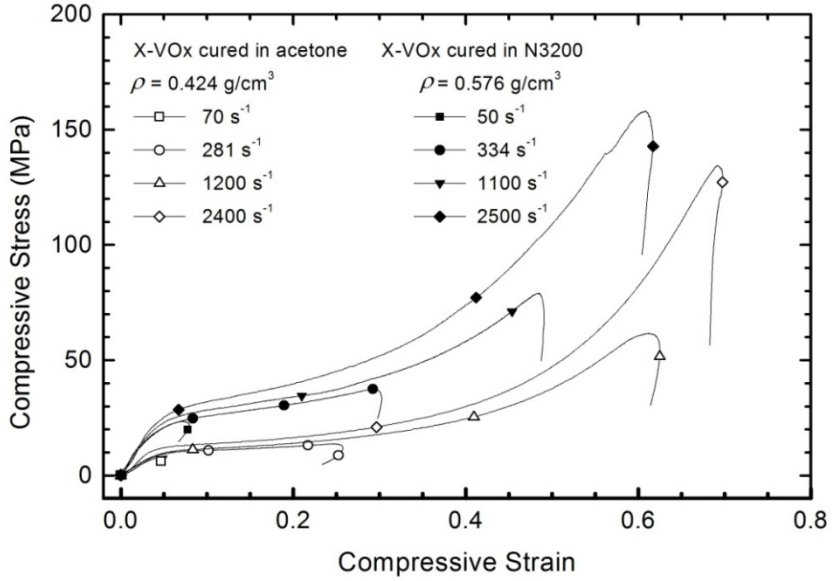

Figure 20: SHPB results at different strain rates showing that the material performed better at higher strain rate than at low strain rate.

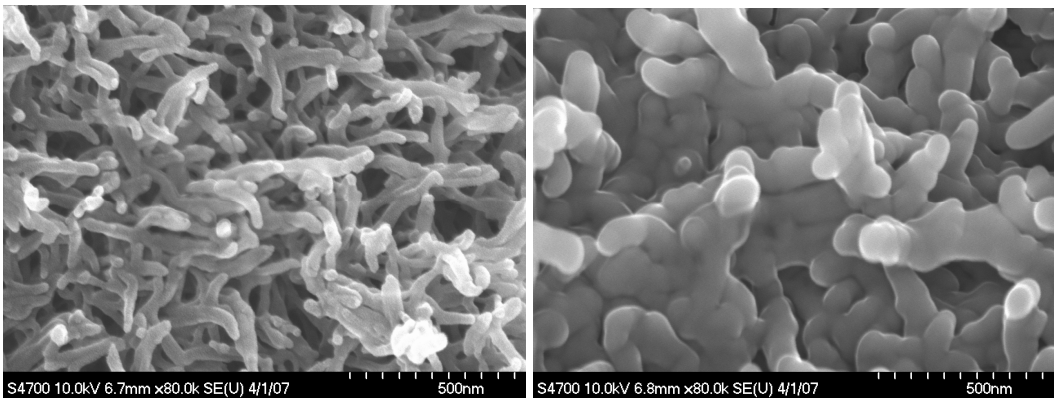

Figure 21: SEM of X-VOx before and after high strain dynamic test using SHPB.

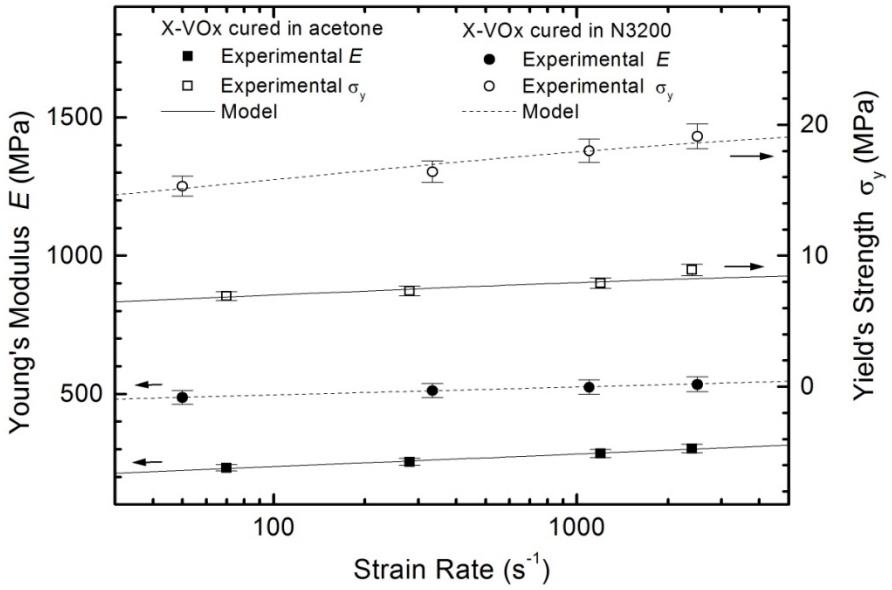

Figure 22: Young's modulus E and yield strength $\sigma_{0.2}$ as a function of strain rates for X-VOx samples

Materials	ρ (g/cm^3)	C_1	C_2	m_1	m_2	σ_0(MPa)	n_1	n_2
X-VOx cured in acetone	0.424	0.50	0.24	0.45	0.083	7.0	1.83	2.03
X-VOx cured in N3200	0.576	0.50	0.50	0.45	0.024	15.9		
CSA (Luo et al, 2006)	0.452	0.81	0.12	0.10	0.40	5.9	3.10	3.10

Table 3: Summary of best fit constants from SHPB results

4.6 High Speed Photography and Digital Image Correlation

A Cordin 550-62 high-speed digital camera was used to acquire images of the sample surface during SHPB tests, for measurements of surface deformations using digital image correlation technique and for observing the failure behavior at high strain rates. Among the total 62 frames, four typical frames are shown in Figure 18. Speckles were firmly made on the specimen surface using black silicone rubber dots so that they would follow the deformation of the sample, even at very high strain levels. A ruler with small grid of 1 × 1 mm was fixed on the base of the SHPB, and was also recorded by the camera for use as the scale of the image. Figure 18(A) shows the image of the specimen prior to loading at time 0 μs. At time 724.0 μs, as shown in Figure 18(D), the specimen with density 0.416 g/cm^3 was compressed by about 55% strain, but did not show any formation of surface cracks despite the high lateral tensile strains, indicating an extremely ductile behavior under high speed impact. It is noted that under quasi-static compression on an MTS system, at ~ 70% compressive strain, X-VOx sample developed surface cracks as shown in Figure 9. In compression at high strain rate, the applied compressive strain was limited by 1.5 ms loading duration of the SHPB so that it did not reach a value high enough to cause formation of large number of surface cracks.

Digital image correlation technique was used to determine the surface strain distribution on a specimen. Each pixel represents a length of 37.04 μm in both horizontal and vertical directions. Surface deformations were determined using Figure 18(A) as the reference image and successive images as deformed images. Seven deformed images acquired at 111.4 μs, 194.9 μs, 250.6 μs, 306.3 μs, 362.0 μs, 417.7 μs and 473.3 μs were processed

using the digital image correlation (DIC). The strains determined from the bar waves, and from DIC (marked by "DIC") are synchronized with the stress determined from the transmitted wave, and are plotted in Figure 19. Under very high compressive strains, as in the case of Figure 18(D), speckles are too close to be discerned so that deformations can no longer be determined from DIC. Consequently the deformed images after Figure 18(D) do not render any data points as determined from DIC. From Figure 19, the data points from DIC agree well with data obtained from analysis of the waves recorded by the strain gages attached to the bars, providing further assurance on the validity of the dynamic compressive data. In Figure 19, also the transverse strain (normal strain in the vertical direction) determined from DIC on 7 images is also plotted with axial strain. The Poisson's ratio was determined from these strains, and the average value is 0.152±0.008, in the regime of nonlinear deformation. The small Poisson's ratio indicates that the material is in general absorbed by its own porosity of the X-VOx so that lateral deformation is minimal.

Figure 20 (A) and (B) show the contour of displacement in the horizontal and transverse direction as determined from DIC on image "D" of Figure 18, respectively. Figure 20 (B) and (D) show the contour of normal strain in the horizontal and transverse direction, respectively. Results show that surface deformations on samples are relatively uniform in the central region, indicating that compaction occurs relatively uniformly throughout the specimen. The average axial compressive strain for the strain field as shown in Figure 20 (C) is 26.74%±0.05%, very close within 2.3% to the strain 26.14% as measured by strain gages attached to the bars.

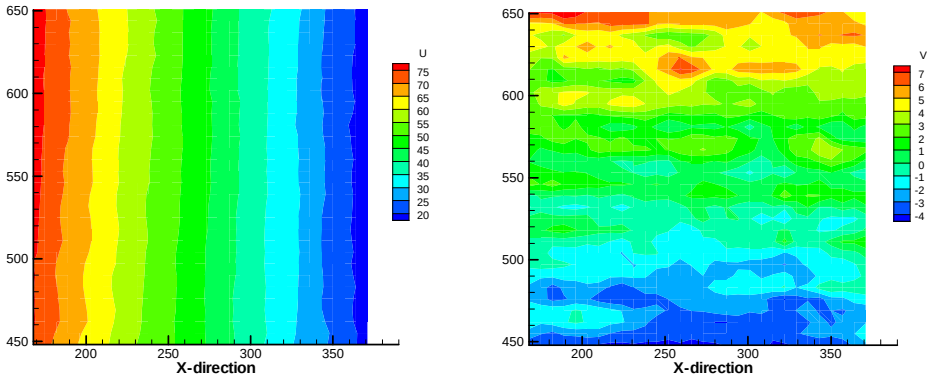

(A) (B)

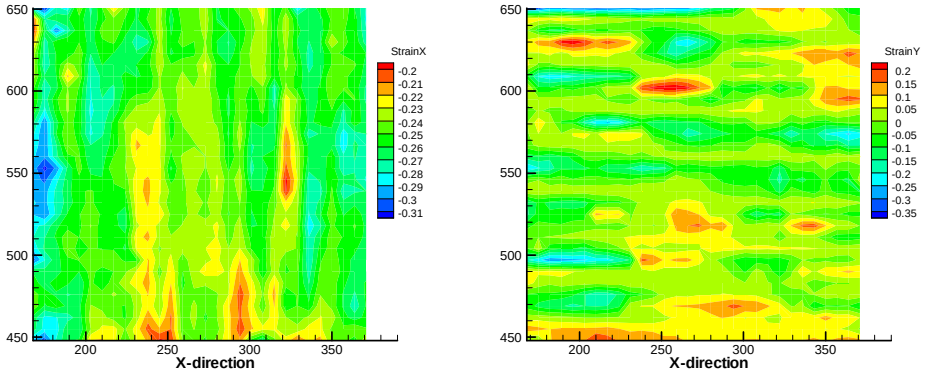

(C) (D)

Figure 23: Contours of displacements and strains of X-VOx cured in acetone (ρ= 0.416 g/cm^3) determined from DIC.

(A) Axial displacement field (Unit: 1 pixel = 37.04 μm); (B) Transverse displacement field (Unit: 1 pixel = 37.04 μm); (C) Axial strain field; (D) Transverse strain field;

4.7 Effect of Mass Density

X-VOx samples with different densities were compressed on the SHPB to determine the effect of density on the stress-strain relations. As it was discussed previously, X-VOx with higher densities was prepared by applying a thicker conformal polymer coating on the skeletal framework, by curing the samples in a N3200 solution rather than pure acetone. Figure 24 shows the stress-strain relations for native VOx and X-VOx samples at four different densities at strain rates close to 300 s^{-1}. It is noted that in dynamic testing, it is difficult to reach exactly the same strain rate because of different experiments. The testing at a strain rate nearly 300 s^{-1} is considered to reveal primarily the effects of density on the stress-strain relationship, although the curve is not complete enough to ultimately fail samples. Results indicate that inducing stress-strain relationship is very sensitive to the mass density at those strain rates. At all densities, the stress-strain curves show similar trends, namely, elastic, compaction followed by plastic hardening and densification. At higher mass densities, X-VOx exhibits higher stiffness and higher strength, giving curves above than those at lower densities. Figure A1 shows the variation of both the Young's modulus and the 0.2% offset compressive yield strength as a function of mass density. Young's modulus and yield strength (or plastic collapse stress) were fitted into the power law relations according Equations (3) and (4)

$$\frac{E}{E_s} = C_3\left(\frac{\rho}{\rho_s}\right)^{n_1} \qquad (3)$$

$$\frac{\sigma}{\sigma_s} = C_4\left(\frac{\rho}{\rho_s}\right)^{n_2} \qquad (4)$$

where E and E_s, σ and σ_s, ρ and ρ_s are Young's modulus, yield strength, and mass density of the corresponding bulk and skeletal material, respectively; C_3 and C_4 are constants and dependent on the material skeletal density while n_1 and n_2 are density exponents and not dependent on the material skeletal density. The modulus and the strength data are fitted into Equation (3) and (4) for a given strain rate (~300 s^{-1}), and the best-fit parameters are listed in Table 3 using E_s = 1GPa, σ_s = 10 MPa, and ρ_s = 1.0 g/cm^3. The fitted curves are plotted with the experimental data as shown in Figure A1. The difference between the experimental data and model is within 5%, indicating a good agreement.

4.8 Effect of Water and Moisture Concentration

The solvent concentration can affect significantly the mechanical behavior of polymers and cross-linked aerogels (Luo, Lu and Leventis, 2006). In this section, we report the effects of water and moisture absorption on the stress-strain relation of X-VOx at high strain rates. Cylindrical samples of X-VOx with 13.25 mm diameter and 36 mm length, and initial mass densities of 0.434 and 0.574 g/cm^3 were tested under ambient conditions immersed in water. Also other X-VOx cylindrical samples with initial mass densities of 0.414 and 0.592 g/cm^3, were placed inside an enclosed container with water present (producing 97±1% relative humidity); these samples did not have direct contact with water. Both the mass and the volume changes of the X-VOx samples were monitored over a period of time, and densitywere calculated from the measured mass and volume, and data are shown Figure A2 and A3, respectively. As shown in Figure A2, when samples were immersed in water, the weight gain reached a steady value in about two

days. When samples were placed under 97±1% relative humidity, the weight gain increased slightly and gradually, and could hardly reach a fully saturated state. Therefore, in order to determine the effect of moisture concentration on the mechanical behavior, we used samples remaining under 97±1% relative humidity for two months. Table 4 summarizes the final densities of X-VOx with presence of water or solvent for four densities of X-VOX under ambient conditions. The water did not escape from the samples after removing from the water container, indicating that water was trapped in the mesopores. The percent weight gain after immersion in water as shown in Figure 23, was higher for X-VOx samples with lower density (e.g. 0.434 g/cm$^{3)}$) than for X-VOx with higher density (e.g. 0.574 g/cm^3). This is the attributed proof that at lower density, the X-VOx samples have higher porosities allowing more water to be trapped in the mesopores. The weight gain of X-VOx samples under 97% relative humidity was much less than that immersed in water, and it did not depend on the initial weight of the samples. This is the attributed proof that the moisture is be absorbed by the polyurea skeletal coating, which absorbs nearly the same percentage of moisture regardless of its thickness. Figure 24 shows the volume change as a function of time, and points out all X-VOx samples shrink both in water and under high humidity. Shrinkage is more servere for X-VOx under moisture than in water. Larger volume shrinkages are observed for X-VOx samples of lower densities. For X-VOx with a density of 0.434 g/cm^3, the volume was reduced by 7.8% in water after 1320 hours, whereas the volume of X-VOx with density of 0.574 g/cm^3 was reduced by 1.8% for the same period. For X-VOx with density of 0.417 g/cm^3 exposed to 97% relative humidity, the volume was reduced by 43% over 1320 hours, whereas X-VOx with density of 0.592 g/cm^3 shrank by only 7.9% during the same time.

These results indicate that X-VOx with high densities thus has thicker polyurea coating over skeletal framework, and tends to allow the worm-like vanadia nanoparticles to form a more stable network resisting dimensional change more effectively. Figure 25 shows the density as a function of time for X-VOx in water or under 97% relative humidity. The density of X-VOx immersed in water increased rapidly in short times, then remaining constant after two days; the density of X-VOx increased by 90% for X-VOx with initial density of 0.574 g/cm^3, and increased by 150% for X-VOx with initial density of 0.434 g/cm^3. The percent mass density increase is higher for samples with lower initial densities (0.417 g/cm^3) than for samples with higher initial densities (0.592 g/cm^3), indicating that more water tends to fill the accessible pores in the former. From Table43, the mass densities of X-VOx samples of two different densities after saturation with water were 1.102 and 1.114 g/cm^3 for samples with initial dry densities of 0.434 g/cm^3 and of 0.574 g/cm^3, respectively, that is very close to each other.

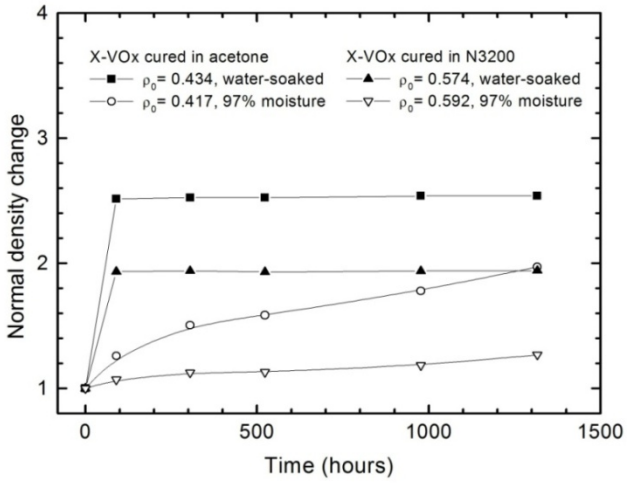

Figure 24: Percent mass gain as a function of time for X-VOx cured in acetone and in N3200

Samples were either fully water saturated or under 97% relative humidity were cut into 2.54 mm thick samples and were tested on the SHPB. Figure 26 compares the stress-strain relations at a strain rate of ~300 s^{-1} for the dry, water-soaked and moisturized samples of X-VOx samples cured in acetone and in N3200, respectively. It is noted that these stress-strain curves is not complete due to SHPB limit at moderate strain rate of ~ 300 s^{-1}, similarly to Section 3.3d (sample did not fail at the end of the testing and deformed with large plastic strain). The shape of stress-strain curves for three kinds of sample are similar. The stress-strain curves for the water-soaked samples are very close to those of dry samples, indicating that water does not have a very significant effect on the mechanical behavior in compression at high strain rates. By the same token, it may be noted that water absorption has a definite effect on the mechanical behavior at low strain rate, 5×10^{-3} s^{-1} (see Figure 12). At low strain rate, water trapped in the mesopores could escape gradually from the sample so that water-soaked X-VOx samples would be weaker than a dry one, indicating partially collapse of the structure. At high strain rates, moisture or water would not escape during very short duration so that water would actually carry partially the applied load allowing the overall mechanical behavior to retain almost unchanged in comparison with the dry samples. The detailed mechanisms for the effects of water and moisture absorption on the mechanical behavior involve complex micro-flow in nano-porous structures and need further investigation. For X-VOx samples with lower initial density (0.417 g/cm^3), samples with weight gain at 97% relative humidity have stress-strain relationships different from those of both water-soaked and dry samples due to associated volume shrinkage and the 90% increase in density. For X-VOx with higher initial density (0.592 g/cm^3), the water absorption weakens only slightly the

mechanical properties at high strain rate, while samples under 97% relative humidity does not have much effect on the mechanical behavior.

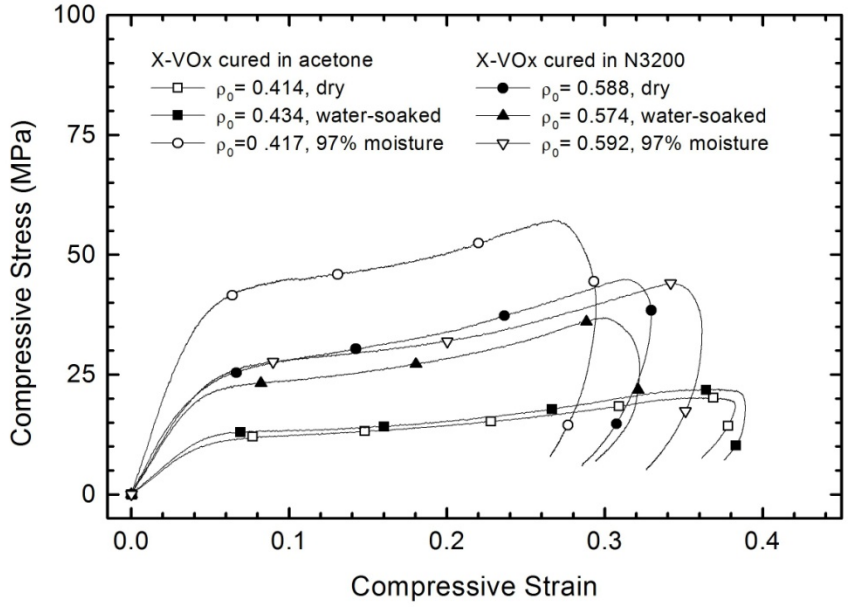

Figure 25: Effect of water and moisture on cross-linked vanadium aerogels

4.9 Effect of Low Temperatures

Samples of X-VOx with 2.54 mm thickness and 12.70 mm diameter were tested on the SHPB with an identical incident pulse used for testing X-VOx samples at a strain rate of ~1300 s^{-1}, same as in Section 3.3a, which cause the samples to fail finally. The compressive stress-strain relations at strain rate ~ 1300 s^{-1} at four temperatures for two densities of X-VOx, (0.417 and 0.546 g/cm^3), are plotted in Figure 27. The Young's modulus and yield strength at each temperature are listed in Table 5. With the decrease in

temperature, mechanical properties such as the yield strength increases by as much as 40% for samples. The Young's modulus (or yield strength) at -170 °C were unchanged (increased by 19%) for X-VOx samples with density 0.417 g/cm^3. For X-VOx samples with density 0.552 g/cm^3, the Young's modulus and the yield strength increased by 44% and 22%, respectively, in comparison with the corresponding values at room temperature. Furthermore, for the temperatures investigated (-170 °C, -55 °C, -5°C, and room temperature), the stress-strain curves tend to fall higher as the temperature decreases, indicating that the X-VOx has superior performance at lower temperatures, a feature not found with most monolithic bulk materials such as metals, polymers, and ceramics which will normally become brittle at low temperatures. This property makes X-VOx a material of choice for energy absorption at low temperatures for application in protection against impact force, such as in armor. For example, rubber behaves like as brittle glass when the temperature decreases to -170 °C, and easily crushed into powder with a slight impact. For low carbon steel, there also exists a critical temperature in range between -40°C to -50°C where the material undergoes the transformation from ductile to brittle. However, 3D stacked nano-fibrous X-VOx, do not show any sign of brittleness when exposed to liquid nitrogen. This indicates that X-VOx exhibits potential structural application in energy absorption under cryogenic environments at high speed impact.

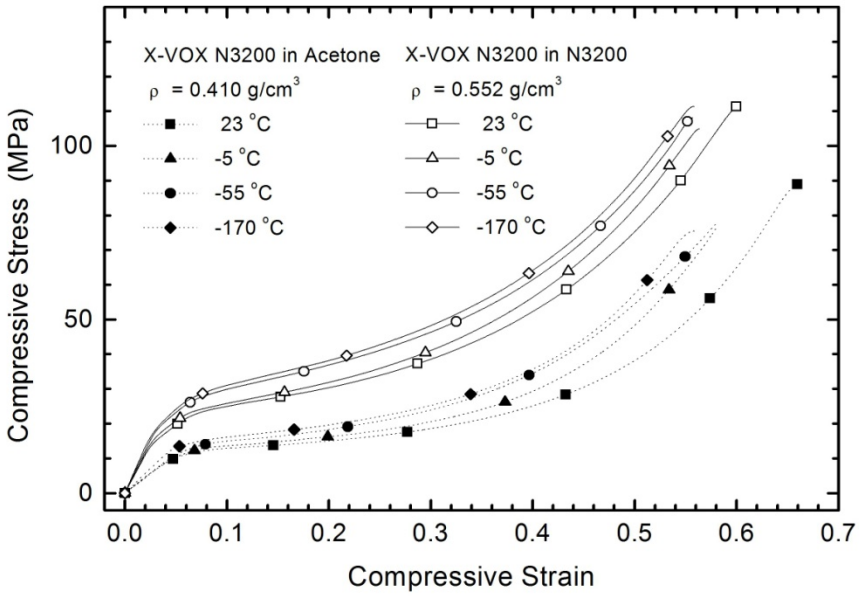

Figure 26: High strain rate compression test at different temperatures.

CHAPTER V

CONCLUSION

A new low-density, highly nano-porous strong lightweight crosslinked vanadium oxide aerogel was developed by conformal nano-encapsulation of the skeletal framework of native vandia aerogel with isocyanate derived polyureas. X-VOx has potential in engineering applications as it has overcome the brittleness and hydrophilicity of native VOx. Native aerogels which are 97% porous, a bulk density of 0.08 g/cm^3 but are too brittle and hydrophilic to be of any significant use. Native vanadium gels were found to contain vanadium (IV) with BET surface areas 216 m^2/g, and consisted of entangled 100-200 nm long, 30-40 nm thick worm-like framework. Infrared spectra of native vanadia aerogels show the strong absorption of V=O bond. TGA analysis shows a loss of ~15% mass at around 100 ^{o}C accompanied by a strong exothermic heat flow by DSC with a peak at 80 ^{o}C. XRD and XPS data shows the chemical $V_3O_7.H_2O$ compound of native VOx with 5-12 nm nanocrystallite, presenting at ~2/3 vanadium (V) and at ~1/3 vanadium (IV). Vanadia wet gel reacted with isocyanates in the mesopores, forming interparticle molecular tethers via urethane groups and urea bridges. TGA shows X-VOx samples contain ~3% w/w moisture, ~82% of isocyanate-derived polymer and a balance of vanadia (15%) for density of about 0.421 g/cm^3. Characterized by ATR-IR spectroscopy, the resulting X-VOx confirms uniform distribution of the polymer. The cross-linker oligmer has been taken conformally to form a 4 nm thick polymer on the native vanadia worm-like skeleton.

Through DMA, a primary glass transition temperature was identified at 118.4 °C. In MTS quasi-static compression, the X-VOx material was weakened after it absorbed water, and the mechanical behavior was found to be not sensitive to low strain rates (4×10^{-4} - 4×10^{-2} s^{-1}). The X-VOX samples have an average yield strength 5.22 MPa, and

an ultimate compressive strength (240~370 MPa) and 80% compressive failure strain and better properties in low temperature, suitable for force protection in armor applications and cryogenic structure application. The compressive behavior of two X-VOx samples at two different densities at high strain rates 50–2500 s^{-1} was investigated using a long split Hopkinson pressure bar (SHPB) developed at Oklahoma State University. The dependence of Young's modulus and 0.2% offset yield strength on the mass density was determined by quantitative relations. The surface full-field deformation of X-VOx samples was determined with digital image correlation on a series of high-speed deformed images on SHPB. The axial deformation was relative uniform and no localized compaction occurred in compression at high strain rates; the Poisson's ratio was determined at 0.152. X-VOx samples failed at about 60-70% strain by axial splitting near lateral surface at high strain rates. Under high strain rates, water absorption affects the mechanical properties of X-VOX less than at low strain rates, and moisture absorption has a more significant effect on the compressive behavior of X-VOx samples with lower densities than with higher ones. At -170 ºC under impact, X-VOx exhibits a well ductile behavior, bending the trend in most existing materials such as monolithic metals, polymers which become brittle at low temperatures.

REFERENCES

Bertino, M.F., Hund, J.F., Zhang, G., Sotiriou-Leventis, C., Tokuhiro, A.T., Leventis, N.: Room temperature synthesis of noble metal clusters in the mesopores of mechanically strong vanadium-polymer aerogel composites. *J. Sol.-Gel. Sci. Technol.*, **2004**, *30*(1), 43–48

Chen, W., Zhang, B., Forrestal, M.J., "A split Hopkinson bar technique for low-impedance material," *Exp. Mech.*, **1999**, *39*(2), 81–85

Chen, W., Lu, F., Cheng, M.: Tension and compression testing of two polymers under quasi-static and dynamic loading. *Polym. Test.*, **2002**, *21*(2), 113–121

Frew, D.J., Forrestal, M.J., and Chen, W.: Pulse-shaping techniques for testing brittle materials with a split Hopkinson pressure bar. *Exp. Mech.*, **2002**, *42*(1), 93–106

Gama, B.A., Lopatnikov, S.L., Gillespie, J.W.: Hopkinson bar experimental technique: A critical review. *Appl. Mech. Rev.*, **2003**, *57*(4), 223–250

Gray, G.T.: Classic split-Hopkinson pressure bar technique. *Mech. Test. Eval.*, **2000**, ASM Handbook *8*, 462–476

Katti, A., Shimpi, N., Roy, S., Lu, H., Fabrizio, E.F., Dass, A., Capadona, L.A., Leventis, N.: Chemical, physical, and mechanical characterization of isocyanate cross-linked amine-modified vanadium aerogels. *Chem. Mater.*, **2006**, *18*(2), 285–296

Knauss, W.G., Zhu, W.: Nonlinearly viscoelastic behavior of polycarbonate. I. Response under pure shear. *Mech. Time-Depend. Mater.*, **2002**, ***6***(3), 231–269

Leventis, N., Sotiriou-Leventis, C., Zhang, G., Rawashdeh, A.M.: Nanoengineering strong vanadium aerogels. *Nano Lett.*, **2002**, *2*(9), 957–960

Leventis, N., Palczer, A., McCorkle, L., Zhang, G., Sotiriou-Leventis, C.: Nanoengineered vanadium polymer composite aerogels with no need for supercritical fluid drying. J. *Sol. Gel. Sci. Technol.,* **2005**, *35*(2), 99–105

Lu, H., Cary, P.D.: Deformation measurements by digital image correlation: Implementation of a second-order displacement gradient. *Exp. Mech*., **2000**, *40*(4), 393–400

Meador, M.A.B., Fabrizio, E.F., Ilhan, F., Dass, A., Zhang, G., Vassilaras, P., Johnston, J.C., Leventis, N.: Crosslinking amine-modified vanadium aerogels with epoxies: Mechanical strong lightweight porous materials. *Chem. Mater*., **2005**, *17*(5), 1085–1098

Pierre, A.C., Pajonk, G.M.: Chemistry of aerogels and their applications. *Chem. Rev*., **2002**, *102*(11), 4243–4265

Woignier, T., Reynes, J., Alaoui, A.H. et al.: Different kinds of structure in aerogels: relationships with the mechanical properties. *J. Non-Cryst. Solids*, **1998**, *241*(1), 45–52

Zhang, G., Dass, A., Rawashdeh, A.M., Thomas, J., Counsil, J.A., Sotiriou-Leventis, C., Fabrizio, E.F., Ilhan, F., Vassilaras, P., Scheiman, D.A., McCorkle, L., Palczer, A., Johnston, J.C., Meador,M.A., Leventis, N.: Isocyanate-crosslinked vanadium aerogel monoliths: Preparation and characterization. *J. Non-Cryst. Solids*, **2004**, *350*, 152–164

U.F. Ilhan, E.F. Fabrizio, L. McCorkle, D. A. Scheiman, A. Dass, A. Palczer, M.B. Meador, J.C. Johnston and N. Leventis, “Hydrophobic monolithic aerogels by nanocasting polystyrene on amine-modified vanadium,” *J. Mater. Chem.*, **2006**, *16*, 3046–3054

L. A. Capadona, M.A.B. Meador, A. Alunni, E.F. Fabrizio, P. Vassilaras, N. Leventis, "Flexible, low-density polymer crosslinked vanadium aerogels, " *Polymer*, **2006**, *47*, 5754-5761

H. Luo, H. Lu and N. Leventis, "The compressive behavior of isocyanate-crosslinked vanadium aerogel at high strain rates," *Mech. Time-Depend. Mater.*, **2006**, *10*, 83–111

F. Chaput, B. Dunn, P. Fuqua and K. Salloux, "Synthesis and characterization of vanadium oxide aerogels," *J. Non-Cryst. Solids,* **1995**, *188*, 11-18

W. Dong, J. S. Sakamoto, B. Dunn, "Electrochemical properties of vanadium oxide aerogels," *Sci. Tech. Adv. Mater.*, **2003**, *4*, 3-11

K. Sudoh and H. Hirashima, "Preparation and physical properties of V_2O_5 aerogel," *J. Non-Cryst. Solids*, **1992**, *147&148*, 386-388

J. Livage, "Sol-gel chemistry and electrochemical properties of vanadium oxide gels," *Solid State Ion.*, **1996**, *86-88*, 935-942

N. Leventis, "Three dimensional core-shell superstructures: mechanically strong aerogels," *Acc. Chem. Res.* **2007**, accepted.

N. Leventis, P. Vassilaras, E. Fabrizio, A. Dass, "Polymer nanoencapsulated rare earth aerogels: chemically complex but stoichiometrically similar core-shell superstructures with skeletal properties of pure compounds," *J. Mater. Chem.* **2007**, *17*, 1502-1508.

Livage, J, "Vanadium pentoxide gels," *Chem. Mater.* **1991**, *3*, 578-593.

G. Sudant, E. Baudrin, B. Dunn, J.M. Tarascon, "Synthesis and electrochemical properties of vanadium oxide aerogels by the freeze-drying process," *J. Electrochem. Soc.* **2004**, *151*, A666-A671.

D.C.M. Dutoit, M. Schneider, P. Fabrizioli, A. Baiker, “Vanadia-silica mixed oxides: Influence of vanadia precursor, drying method and calcination temperature on structural and chemical properties,” *J. Mater. Chem.* **1997**, *7*, 271-278.

License Information

License Number	2320241378569
License date	Dec 01, 2009
Licensed content publisher	Springer
Licensed content publication	Journal of Sol-Gel Science and Technology
Licensed content title	Synthesis and characterization of the physical, chemical and mechanical properties of isocyanate-crosslinked vanadia aerogels
Licensed content author	H. Luo, **G. Churu**, E. F. Fabrizio ,J. Schnobrich , A. Hobbs A. Dass ,S. Mulik ,Y. Zhang , B. P. Grady, A. Capecelatro, C. Sotiriou-Leventis , H. Lu ,N. Leventis
Licensed content date	Nov 1, 2008
Volume number	48
Issue number	1
Type of Use	Thesis/Dissertation
Portion	Full text
Number of copies	1
Author of this Springer article	Yes and you are a contributor of the new work
Title of your thesis / dissertation	Synthesis, Mechanical and Chemical Characterization of Vanadium based Aerogels
Expected completion date	Dec 2009
Estimated size(pages)	77
Total	0.00 USD

VITA

Habel Gitogo Churu

Candidate for the Degree of

Master of Science
Mechanical Engineering

Thesis: SYNTHESIS AND CHEMICAL, PHYSICAL AND MECHANICAL CHARACTERIZATION OF VANADIUM- BASED AEROGELS

Major Field: Mechanical Engineering

Biographical:

Education:
Completed Bs. in Mechanical engineering technology at OSU, Dec1999
Completed Bs in Mechanical engineering at OSU, May 2004
Completed MS in mechanical engineering at OSU, December 2009

Experience:
Teaching assistant
Research assistant

Name: Habel Gitogo Churu Date of Degree: December, 2009

Institution: Oklahoma State University Location: Stillwater, Oklahoma

Title of Study: SYNTHESIS, MECHANICAL AND CHEMICAL, CHARACTERIZATION OF VANADIUM- BASED AEROGELS

Pages in Study: 62 Candidate for the Degree of Master of Science

Major Field: Mechanical Engineering

Scope and Method of Study:

This study consisted of material synthesis of Vanadium based aerogels, chemical and mechanical analysis and testing to determine possible applications for light weight structural as well as dual purpose applications.

Findings and Conclusions:

A new low-density, highly nano-porous strong lightweight cross-linked vanadium oxide aerogel was developed by conformal nano-encapsulation of the skeletal framework of native vandia aerogel with isocyanate derived polyureas. X-VOx has potential in engineering applications as it has overcome the brittleness and hydrophilicity of native VOx. Native aerogels which were 97% porous, with bulk density of 0.08 g/cm^3 are too brittle and hydrophilic to be of any significant use. The X-VOX samples have an average yield strength 5.22 MPa, and an ultimate compressive strength (240~370 MPa) and 80% compressive failure strain and better properties in low temperature, suitable for force protection in armor applications and cryogenic structure application. The compressive behavior of two X-VOx samples at two different densities at high strain rates 50–2500 s^{-1} was investigated using a long split Hopkinson pressure bar (SHPB) developed at Oklahoma State University. The surface full-field deformation of X-VOx samples was determined with digital image correlation on a series of high-speed deformed images on SHPB. The axial deformation was relative uniform and no localized compaction occurred in compression at high strain rates; the Poisson's ratio was determined at 0.152. X-VOx samples failed at about 60-70% strain by axial splitting near lateral surface at high strain rates. Under high strain rates, water absorption affects the mechanical properties of X-VOX less than at low strain rates, and moisture absorption has a more significant effect on the compressive behavior of X-VOx samples with lower densities than with higher ones. At -170 ^oC under impact, X-VOx exhibits ductile behavior, bending the trend in most existing materials such as monolithic metals and polymers which become brittle at low temperatures.

ADVISER'S APPROVAL: Hongbing Lu